

Semiannual Progress Report

For Stimul-Responsive Polymers with Enhanced Efficiency in Reservoir Recovery Processes

For the work performed during the period of

March 1, 2003 through August 31, 2003

by

Charles McCormick

and

Roger Hester

Issued on September 29, 2003

DOE Award Number DE-FC26-01BC15317

The University of Southern Mississippi
Department of Polymer Science
P.O. Box 10076
Hattiesburg, MS 39406

TABLE OF CONTENTS

Executive Summary	6
TASK 1: Polymer Synthesis	7
Synthetic Cyclo Copolymers with Sulfobetaine Functionality	7
Background	7
Experimental	8
Results and Discussion	12
Conclusion	31
TASK 5: Polymer Solution Mobility	33
Introduction	33
Experimental	35
Results and Discussion	38
Conclusion	45
Nomenclature	46
References	47

FIGURES, SCHEMES, AND TABLES

Figure 1. ^1H NMR spectrum 3-(N,N-diallyl-N-methyl ammonio) propane sulfonate (DAMAPS) in D_2O . R = 3-(trimethylsilyl)-1-propanesulfonic acid, sodium salt as a reference.	13
Figure 2. ^{13}C NMR and DEPT135 spectra of 3-(N,N-diallyl-N-methyl ammonio) propane sulfonate (DAMAPS) in D_2O . R = 3-(trimethylsilyl)-1-propanesulfonic acid, sodium salt as a reference.	13
Figure 3. Representative inverse gated decoupled ^{13}C NMR spectra of the DADMAC-co-DAMAPS cyclocopolymers in D_2O (1M NaCl). (R = 3-(trimethylsilyl)-1-propanesulfonic acid, sodium salt as a reference.)	15
Figure 4. Representative inverse gated decoupled ^{13}C NMR spectra of the DAMA-co-DAMAPS cyclocopolymers in D_2O (1M NaCl, pH=4.0). (R = 3-(trimethylsilyl)-1-propanesulfonic acid, sodium salt as a reference.)	16
Figure 5. Mol% sulfobetaine incorporation as a function of mol % sulfobetaine in the feed as determined by inverse gated decoupled ^{13}C NMR.	17
Figure 6. Mol% sulfobetaine incorporation in DAMA-co-DAMAPS copolymers as a function of mol% sulfobetaine in the feed as determined by inverse gated decoupled ^{13}C NMR.	18
Figure 7. Reduced viscosity as a function of polymer concentration for the homopolymer of DADMAC and copolymers of DADMAC and DAMAPS in deionized water ($T = 25^\circ\text{C}$, $\gamma = 5.96 \text{ s}^{-1}$).	21
Figure 8. Apparent viscosity for the homopolymer of DADMAC and three copolymers of DADMAC and DAMAPS as functions of NaCl and polymer concentrations ($T = 25^\circ\text{C}$, $\gamma = 5.96 \text{ s}^{-1}$).	22

Figure 9. Apparent viscosity for DADS40 and DADS55 as functions of NaCl and polymer concentrations ($T = 25^{\circ}\text{C}$, $\gamma = 5.96 \text{ s}^{-1}$) (● Represents regions of macroscopic phase separation.)	23
Figure 10. Optical micrographs of aqueous solutions of DADS55 in (A) 0.1 and (B) 0.5 M NaCl ($T = 25^{\circ}\text{C}$, $[\text{DADS55}] = 1.0 \text{ g/dl}$).	23
Figure 11. Hydrodynamic radius of DADS40 as functions of NaCl and polymer concentrations ($T = 25^{\circ}\text{C}$).	24
Figure 12. Proposed polymer conformational changes for copolymers of DADMAC and DAMAPS as a function of NaCl concentration.	25
Figure 13. Potentiometric and turbidimetric titrations of DAMA and three copolymers of DAMA and DAMAPS (α represents the degree of ionization of the DAMA mer unit).	27
Figure 14. Apparent viscosity for the homopolymer of DAMA and three copolymers of DAMA and DAMAPS as functions of polymer concentration and the degree of ionization of the DAMA mer unit (α) ($T = 25^{\circ}\text{C}$, $\gamma = 5.96 \text{ s}^{-1}$).	28
Figure 15. Equilibrium surface tension for DAMA and DAMS44 polymers as a function of polymer concentration at selected degrees of ionization of the DAMA mer units (α) ($T=25^{\circ}\text{C}$).	29
Figure 16. Binding isotherms for DAMA and <i>p</i> -cresol (A) and the corresponding hydrodynamic diameter of the polymer-foulant complex (B) as a function of <i>p</i> -cresol concentration and the degree of ionization of the DAMA mer unit (α) ($[\text{DAMA}]=0.2 \text{ g/dl}$; $T=25^{\circ}\text{C}$).	30
Figure 17. Binding isotherms for DAMS44 and <i>p</i> -cresol (A) and the corresponding hydrodynamic diameter of the polymer-foulant complex (B) as a function of <i>p</i> -cresol concentration and the degree of ionization of the DAMA mer unit (α) ($[\text{DAMS44}]=0.2 \text{ g/dl}$; $T=25^{\circ}\text{C}$).	31
Figure 18. Repeat unit structures in acrylamide copolymers. AM is acrylamide, AMPS is 2-acrylamido-2-methylpropanesulfonate, AMBA is 3-acrylamido-3-methylbutanoate, and APTAC is 3-acrylamidopropyltrimethylammonium	37
Figure 19. Plot of normalized intrinsic viscosity vs. screening length to charge spacing. Filled circles and solid trend line represent high molecular weight data from the literature. Small open circles and dotted trend line represent low molecular weight data from the literature. Various symbols and dash-dot trend line represent data collected in our laboratory for acrylamide copolymers as identified in Table 7.	39
Figure 20: Literature Data and Flory Fit Lines	42
Figure 21: Laboratory Data and Flory Fit Lines	44
Scheme 1. Synthetic pathway for preparation of 3-(N,N-diallyl-N-methyl ammonio) propane sulfonate (DAMAPS)	12
Scheme 2. Synthetic pathway for preparation of DADMAC-co-DAMAPS cyclocopolymers.	14
Scheme 3. Synthetic pathway for preparation of DAMA-co-DAMAPS cyclocopolymers	16

Table 1.	Reaction parameters and polymer composition for the copolymerization of DADMAC (M_1) and DAMAPS (M_2)	18
Table 2.	Reaction parameters and polymer composition for the copolymerization of DAMA (M_1) and DAMAPS (M_2)	19
Table 3.	Microarchitectural Analysis: Distribution of Monads, Dyads and Triads per 100 Repeats as a Function of the Monomer Feed Ratio ($M_1:M_2$)	19
Table 4.	Classical light scattering data for the copolymers of DADMAC (M_1) with DAMAPS (M_2) in 1 M NaCl	20
Table 5.	Classical light scattering data for the copolymers of DAMA (M_1) with DAMAPS (M_2). Experimental Information	20
Table 6.	Rejection Ratios as a function of $[\text{Cresol}]_{\text{feed}}$, and pH for DAMA and DAMS44.	32
Table 7.	Experimental Information for Laboratory Data	43
Table 8.	Experimental Information for Literature Data	43

Disclaimer

This report was prepared as an account of work sponsored by an agency of the United States Government. Neither the United States Government nor any agency thereof, nor any of their employees, makes any warrant, express or implied, or assumes any legal liability or responsibility for the accuracy, completeness, or usefulness of any information, apparatus, product, or process disclosed, or represents that its use would not infringe privately owned rights. Reference herein to any specific commercial product, process, or service by trade name, trademark, manufacturer, or otherwise does not necessarily constitute or imply its endorsement, recommendation, or favoring by the United States Government or any agency thereof. The views and opinions of authors expressed herein do not necessarily state or reflect those of the United States Government or any agency thereof.

Abstract

A sulfobetaine monomer, 3-(*N,N*-diallyl-*N*-methyl ammonio) propane sulfonate, has been synthesized and copolymerized with *N,N*-diallyl-*N,N*-dimethylammonium chloride and *N,N*-diallyl-*N*-methyl amine. ^{13}C NMR analysis indicates that the resulting polymers maintain the five-membered ring structure common to cyclopolymerized diallylammonium salts. The solution behavior of the DADS series is dictated by two opposing forces: cationic charge-charge repulsion along the polymer backbone from DADMAC mer units, and the dipole-dipole attractive forces created by the presence of the sulfobetaine DAMAPS unit. Stimuli-responsive behavior including phase separation can be realized by adjusting ionic strength. For the DADS series, reactivity ratio studies indicate random incorporation of the two mer units with a slight tendency towards favored incorporation of the sulfobetaine. Turbidimetric titration, low-shear viscosity, and equilibrium surface tension experiments were utilized to study the solution behavior of the resulting copolymers. At high degrees of ionization, the copolymers assume an expanded conformation due to the charge-charge repulsions along the copolymer backbone. As the molar incorporation of the sulfobetaine increases (at high degrees of ionization), the copolymer assumes a more relaxed conformation due to dipole-dipole interactions. As the degree of ionization of the tertiary amine decreases, hydrophobic associations dominate the solution behavior. For copolymers with low incorporation of sulfobetaine, chain collapse leading to precipitation occurs. However, at higher incorporations, the sulfobetaine acts as a hydrophilic segment to limit hydrophobic packing and minimizes the chain collapse. Equilibrium dialysis experiments have demonstrated that the DAMA-based copolymers may be utilized in a micellar-enhanced ultrafiltration application. A facile mechanism of foulant capture and release is provided by the pH-reversible domains.

In this report, we continue to study polymer solution theory to account for the electrostatic interactions present in solutions of charged polymers. Polymers with ionic charges are referred to as polyions or polyelectrolytes. Both a modified Flory model and OSF model were studied for their predictive capabilities using both past and present polyelectrolyte solution data. The OSF model appears superior in providing a universal relationship correlating polyion solution intrinsic viscosities with solution conditions and polymer structures.

EXECUTIVE SUMMARY

To date, our synthetic research efforts have been focused on the development of stimuli-responsive water-soluble polymers designed for use in enhanced oil recovery (EOR) applications. These model systems are structurally tailored for potential application as viscosifiers and/or mobility control agents for secondary and tertiary EOR methods. The goal of previous synthetic work has been to design novel polymers that exhibit large dilute solution viscosities in the presence of the adverse conditions normally encountered in oil reservoirs (such as high salt concentrations, the presence of multivalent ions, and elevated temperatures). The polymers are also designed to have “triggerable” properties that can be elicited by external stimuli, such as changes in pH and/or salt concentration.

Previously, we have investigated polyelectrolytes (i.e. polyampholytes and polybetaines) and hydrophobically modified polyelectrolytes as potential viscosifiers for EOR applications. The polyelectrolytes demonstrate remarkable salt tolerance due to their amphoteric nature, while the hydrophobically modified (HM) polyelectrolytes exhibit improved viscosification as a result of intermolecular hydrophobic association, which imparts an additional viscosification mechanism to the polymers. This current research is focused on combining the benefits of polyelectrolytes and hydrophobic modification in the same polymer system. Ideally, the HM polyelectrolytes will exhibit a unique combination of the stimuli-responsive behaviors observed in previously examined systems.

Another goal of this research is to investigate the interaction of surfactants with the HM polyelectrolytes. Surfactants are critical components in micellar enhanced EOR (e.g. polymer-surfactant flooding) processes because of their ability to reduce interfacial tension and mobilize oil trapped in reservoir formations. We aim to synthesize polymer systems that will demonstrate synergistic increases in solution viscosity upon the addition of surfactants. Such polymer systems may demonstrate superior performance as mobility control agents in micellar enhanced EOR processes due to surfactant-induced viscosity enhancement.

Experience has shown that efficient polymers for oil recovery must have a large hydrodynamic coil size in solution as they flow through the reservoir. Larger polymer coils have higher extensional viscosities, which lower aqueous phase mobility in the porous media, and thereby improve sweep efficiency to displace residual reservoir oil. Ideally, the macromolecules should have a collapsed coil configuration during injection into the reservoir to reduce both pumping costs and shear degradation at the well-head. Also, polymer coils should expand after injection to increase their solution extensional viscosity within the reservoir. The desired complex solution behavior may be achieved with synthetic polymers that can change their macromolecular conformation upon encountering certain environmental stimuli such as variations in solution temperature, pH, and electrolyte concentration.

In this report, we expand polymer solution theory to account for the electrostatic interactions present in solutions of charged polymers. Polymers with ionic charges are referred to as polyions or polyelectrolytes. Findings presented in this report will facilitate the design of new polyelectrolytes for improved sweep efficiency during polymer flooding. The OSF theory of polyelectrolyte solutions was found to be useful for correlating behavior with respect to charges in solution salt concentration.

Task 1: Polymer Synthesis

Background

To date, our synthetic research efforts have been focused on the development of stimuli-responsive water-soluble polymers designed for use in enhanced oil recovery (EOR) applications. These model systems are structurally tailored for potential application as viscosifiers and/or mobility control agents for secondary and tertiary EOR methods. The goal of previous synthetic work has been to design novel polymers that exhibit large dilute solution viscosities in the presence of the adverse conditions normally encountered in oil reservoirs (such as high salt concentrations, the presence of multivalent ions, and elevated temperatures). The polymers are also designed to have “triggerable” properties that can be elicited by external stimuli, such as changes in pH and/or salt concentration.

Various zwitterionic polymers have been investigated in our laboratories due to their unique responsiveness to saline media.¹ Unlike polyelectrolytes (PEs), which bear *either* anionic or cationic charges, polyzwitterions (PZs) bear *both* anionic and cationic functionalities. PZs may be categorized as polyampholytes (anionic and cationic charges on *separate* repeat units) or polybetaines (anionic and cationic charges on the *same* repeat unit). In aqueous solution, PEs generally collapse with increasing ionic strength due to the screening of intramolecular repulsions between like charges along the polymer backbone.² This phenomenon, known as the polyelectrolyte effect, tends to impair the performance of PEs in applications where the polymers encounter saline media. In contrast to PEs, PZ solutions exhibit an antipolyelectrolyte effect in which the polymer adopts a more expanded conformation with increasing ionic strength.³ This effect is attributed to the screening of intramolecular attractions between the pendant anionic and cationic moieties along the polymer backbone by the small molecule electrolytes. The increase in hydrodynamic size is also accompanied by an increase in solution viscosity, making PZs ideal candidates for salt-tolerant viscosifiers.

Polyzwitterions containing the sulfonate functionality have been thoroughly studied beginning with the pioneering work of Hart and Timmerman.⁴ In that work, zwitterionic monomers were prepared by the reaction of 2- and 4-vinylpyridine with 1,4-butanedisulfonate. Polysulfobetaines are typically insoluble in deionized water and require a relatively high content of hydrophilic comonomer or the addition of a critical concentration of electrolyte to achieve solubility and viscosity enhancement. Polysulfobetaines have also been synthesized from acrylic,⁵⁻¹² acrylamido,¹³⁻¹⁴ and vinyl imidazolium¹⁵⁻¹⁷ monomers and more recently polysulfobetaine block copolymers have been reported.¹⁸⁻¹⁹

Another area of interest in our laboratories is the synthesis of hydrophobically modified (HM) water-soluble polymers via micellar copolymerization and their solution behavior in aqueous media. These hydrophilic copolymers contain small amounts (typically ≤ 1 mol %) of hydrophobic comonomers that enable viscosification through intermolecular hydrophobic associations.²⁰ Often referred to as associative thickeners (ATs), the HM copolymers exhibit greater thickening efficiency and more complex rheological properties compared to their unmodified counterparts. Several polymer systems investigated by our group have proven to be effective ATs with pH- and shear-responsive behavior.²¹⁻²⁷ Both the PZs and the ATs that have

been the focus of our investigations demonstrate extremely high potential for application in areas such as enhanced oil recovery, drag reduction, coatings, personal care, and cosmetics.

In addition to ATs, hydrophobically modified polymers demonstrating surfactant-like qualities have been the subject of considerable research²⁷⁻³¹ beginning with the classical studies of Strauss.³²⁻³⁵ From the work of many researchers, the nature of hydrophobic associations has been shown to be dictated by many factors including, but not limited to polymer microstructure,³⁶⁻⁴¹ the ‘bulkiness’ of the hydrophobe,⁴²⁻⁴⁵ and the chemical composition of the hydrophobe, i.e. (hydrocarbon vs. fluorocarbon).⁴⁶⁻⁴⁷

In order to obtain an understanding of how the rigidity of the polymer backbone affects the hydrophobic associations of a polysoap, we reported the synthesis and solution behavior of a series of hydrophobically modified cationic quaternary ammonium polyelectrolytes.⁴⁸ In that work, consistent with other reports,⁴⁹⁻⁵¹ we demonstrated that the introduction of long hydrophobic side chains along the backbone of cationic quaternary ammonium cyclopolymers can result in the formation of polymeric micelles or polymeric aggregates under specified conditions. However, the structures that were formed did not demonstrate environmental responsiveness that would be required for an ideal remediative polymer.

This report discloses the synthesis and characterization of a series of copolymers based upon the copolymerization of *N,N*-diallyl-*N,N*-dimethyl ammonium chloride (DADMAC) with the sulfobetaine monomer, 3-(*N,N*-diallyl-*N*-methyl ammonio) propane sulfonate (DAMAPS). These monomers undergo an intramolecular-intermolecular cyclopolymerization yielding five-membered rings and a cationic charge common to polymerized diallyl ammonium salts, as first discovered by Butler.⁵²⁻⁵⁴ The purpose of the present work is to elucidate the compositional effects of zwitterionic comonomer incorporation on the aqueous solution properties of the resulting polyelectrolytes. In particular, the solution behavior as a function of concentration and added electrolytes has been studied by viscometric and dynamic light scattering methods. The results are compared to aqueous solution behavior typically exhibited by polyelectrolytes and polyampholytes

In addition to the research with the previously mentioned zwitterionic polymers, the study was expanded to include the synthesis and solution properties of cyclopolymers of *N,N*-diallyl-*N*-methyl amine (DAMA) and 3-(*N,N*-diallyl-*N*-methyl ammonio) propane sulfonate (DAMAPS). By utilizing turbidimetric titrations, steady-shear viscometry, and equilibrium surface tension, we have examined how the incorporation of the pH-responsive hydrophobic monomer enables the precise control of the polymer conformation in aqueous media. In addition, we examine the effects on the associative properties of the hydrophobe by the incorporation of the zwitterionic sulfobetaine moiety.

Experimental

Materials

All reagents were purchased from Aldrich Chemical Company and used as received unless otherwise noted. DAMA was obtained via previously reported literature procedure.³⁹

Monomer Synthesis

Synthesis of 3-(N,N-Diallyl-N-Methyl Ammonio) Propane Sulfonate (DAMAPS)

N,N-diallyl-*N*-methylamine (DAMA) (0.45 mol) and 1,3-propanesultone (0.5 mol) were reacted in 200 ml acetonitrile with stirring at room temperature for 5 hours. During this period, the product formed as a white precipitate. This was then filtered and washed with three 200 ml aliquots of diethyl ether. DAMAPS was obtained in 72 % yield. M.p. 169-170°C Analysis for C₁₀H₁₉NSO₃. Calculated: C, 51.48 %; H, 8.21 %; N, 6.00 %; S, 13.74 %. Found: C, 51.59 %; H, 8.10 %; N, 5.89 %; S, 13.64 %.

Polymer Synthesis

Synthesis of Copolymers of DAMAPS with DADMAC.

Homopolymers of DAMAPS, DADMAC, and the copolymers of DAMAPS with DADMAC were synthesized by free radical photopolymerization in a 0.5 M aqueous NaCl solution under a nitrogen atmosphere at 35°C using 0.3 mol % 2-hydroxy-1-[4-(hydroxyethoxy)phenyl]-2-methyl-1-propanone (Irgacure 2959) (Ciba) as the photoinitiator. The feed ratio of DADMAC/DAMAPS was varied from 100/0 to 0/100 mol% with the total monomer concentration held constant at 2.5 M. 0.5 M NaCl was maintained in the reaction medium to insure that polymers with high DAMAPS content remained soluble during polymerization. The polymerizations were carried out in a Rayonet photoreactor (Southern New England Ultraviolet Company) operating at 300 nm for 4hr under a nitrogen atmosphere. A low conversion sample was obtained for reactivity ratio studies. The reaction was usually terminated at <50 % conversion as a precaution against copolymer drift. The copolymers were purified by dialyzing against deionized water with 6000-8000 MWCO dialysis tubing (Spectrapor). The dialysis was carried out for two weeks with frequent changing of the permeate. The copolymers were recovered by lyophilization. Conversions were determined gravimetrically.

Synthesis of Copolymers of DAMA with DAMAPS.

Homopolymers of DAMA, DAMAPS, and the copolymers of DAMA with DAMAPS were synthesized by free radical photopolymerization in a 0.5 M aqueous NaCl solution (pH = 4.0) under a nitrogen atmosphere at 35°C using 0.3 mol % 2-hydroxy-1-[4-(hydroxyethoxy)phenyl]-2-methyl-1-propanone (Irgacure 2959) (Ciba) as the photoinitiator. The feed ratio of DAMA/DAMAPS was varied from 100/0 to 0/100 mol% with the total monomer concentration held constant at 2.5 M. 0.5 M NaCl was maintained in the reaction medium to insure that polymers with high DAMAPS content remained homogeneous during polymerization. The pH of the reaction medium was adjusted to 4.0 to ensure protonation of the tertiary amine to facilitate the intermolecular-intramolecular propagation mechanism common to diallyl ammonium salts. The polymerizations were carried out in a Rayonet photoreactor (Southern New England Ultraviolet Company) operating at 300 nm for 4hr. A low conversion sample was obtained for reactivity ratio studies. The reaction was usually terminated at <50 % conversion as a precaution against copolymer drift. The copolymers were purified by dialyzing against

deionized water with 6000-8000 MWCO dialysis tubing (Spectrapor). The dialysis was carried out for two weeks with frequent changing of the permeate. The copolymers were recovered by lyophilization. Conversions were determined gravimetrically.

Instrumentation and Analysis

Elemental Analysis

Elemental analysis was performed by MHW Laboratories, Phoenix AZ. Carbon, hydrogen, nitrogen, and sulfur analyses were performed with a reported accuracy of <0.2%.

^1H and ^{13}C NMR Spectroscopy

^1H and ^{13}C NMR spectra were recorded with a Bruker AC-300. ^{13}C NMR spectra of the cyclocopolymers were obtained at 50.3 MHz using 10-15 wt% 1.0M NaCl aqueous (D_2O) polymer solutions with 3-(trimethylsilyl)-1-propanesulfonic acid, sodium salt DSS as a reference. DEPT135 experiments confirmed peaks assignments for both monomer and polymer samples. A recycle delay of 8 s, 90° pulse length, and inverse gated decoupling to remove all NOE were used for quantitative spectral analysis. Experimental error for the inverse gated decoupled ^{13}C NMR was <5%.

Classical Light Scattering

Molecular weight studies were performed with a Brookhaven Instruments 128-channel BI-2030 AT digital correlator using a Spectra Physics He-Ne Laser operating at 632.8 nm. Weight average molecular weights (M_w) were determined through analysis of the Berry plots.⁵⁵⁻⁵⁷ Hydrodynamic radii were determined using the cumulants analysis of the autocorrelation function obtained at 90° . Refractive index measurements were carried out using a Chromatix KMX-16 differential refractometer.

Potentiometric Titration

Potentiometric titrations were conducted with an Orion 950 Ross[®] FASTQC[™] Titrator with an Orion Ross[®] Sure-Flow semi-micro combination pH electrode (Model 8175BN) under a nitrogen atmosphere. Experimental error for all pH values was ± 0.05 .

Solution Rheology

Dilute solution viscometric studies were conducted with a Contraves LS-30 low-shear rheometer at a constant shear rate of 5.96s^{-1} at 25°C . The reported viscosities were the average of five measurements.

Surface Tensiometry

A Kruss K12 Processor Tensiometer was utilized to conduct Wilhemy plate surface tension measurements. Doubly distilled water (surface water) was used to prepare all surface tension solutions. Reported data was obtained at 25°C as a function of polymer concentration.

Turbidimetry

Turbidity was monitored during the titration with a Brinkmann PC800 Colorimeter.

Copolymer Composition Analysis

Copolymer compositions were determined by inverse gated decoupled ^{13}C NMR according to Equation 1, where I_i , I_a , I_e , I_b , I_f , I_c , and I_g represent the integrated intensities corresponding to carbons i , a , e , b , f , c , and g respectively.

$$\text{Mol\% DAMAPS (M2)} = \frac{2I_i}{3} \left(\frac{1}{I_a + I_e} + \frac{1}{I_b + I_f} + \frac{1}{I_c + I_g} \right) \quad (1)$$

Equilibrium Dialysis Experiments

Equilibrium dialysis experiments were performed utilizing equilibrium dialysis cells (5 ml) from Bel-Art Products and regenerated cellulose membranes having a nominal molecular weight cutoff of 6000. Solutions containing the polymeric surfactant and p-cresol of known concentrations ($[\text{Polymer}] = 0.2\text{g/dl}$; $[\text{Cresol}]_{\text{feed}} = 7\text{mM} - 70\text{mM}$) and known pH (pH=4.5, 7.5, 8.5, or 9.5) were placed in one side of each dialysis cell (retentate) and deionized water (pH adjusted to 4.5, 7.5, 8.5, or 9.5) was placed in the other side (permeate). The cells were thermostated at 25°C in a Napco incubator. The concentration of p-cresol in the retentate, $[\text{Cresol}]_{\text{ret}}$ and permeate, $[\text{Cresol}]_{\text{per}}$ were determined by UV spectroscopy after a 24 hour period. (Dialysis experiments in the absence of polymer indicated that equilibrium concentrations of p-cresol were obtained in 24 hr). Dynamic light scattering data indicated that the polymeric surfactant was quantitatively retained within the retentate compartment.

Analysis of Equilibrium Dialysis Experiments.

From $[\text{Cresol}]_{\text{ret}}$ and $[\text{Cresol}]_{\text{per}}$, the concentration of p-cresol bound within the hydrophobic microdomains of the polymeric surfactant, $[\text{Cresol}]_{\text{bnd}}$, was calculated from Equation 2.

$$[\text{Cresol}]_{\text{bnd}} = [\text{Cresol}]_{\text{ret}} - [\text{Cresol}]_{\text{per}} \quad (2)$$

Equation 2 remains valid if the concentration of cresol in the permeate is equivalent to the free concentration of cresol (unbound cresol) in the retentate. From the concentration of bound cresol, the ratio of moles of cresol bound per mole of polymer, r , is then calculated from equation 3:

$$r = \frac{[Cresol]_{bnd}}{[Polymer]} \quad (3)$$

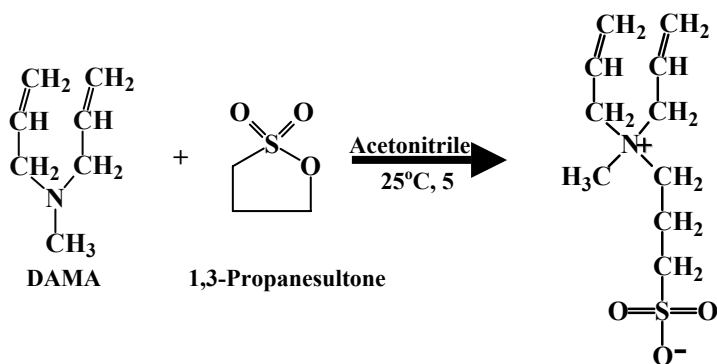
where [Polymer] is the concentration of polymer in the retentate. Binding isotherms were constructed by plotting r as a function of free cresol in the retentate, $[Cresol]_{free}$.⁵⁸⁻⁵⁹ Efficiency of foulant sequestration is analyzed by monitoring rejection ratios,⁶⁰ a term commonly used in membrane applications which is given in equation 4:

$$\text{Rejection Ratio} = \left(1 - \frac{[Cresol]_{per}}{[Cresol]_{ret}} \right) \times 100 \quad (4)$$

Results and Discussion

Monomer Synthesis

3-(*N,N*-diallyl-*N*-methyl ammonio) propane sulfonate (DAMAPS) was synthesized by the ring opening reaction of 1,3-cyclopropanesultone with *N,N*-diallyl-*N*-methylamine as shown in Scheme 1. Monomer structure was confirmed by elemental analysis, ¹H, ¹³C NMR and DEPT135 as shown in Figures 1 and 2.



Scheme 1. Synthetic pathway for preparation of 3-(*N,N*-diallyl-*N*-methyl ammonio) propane sulfonate (DAMAPS).

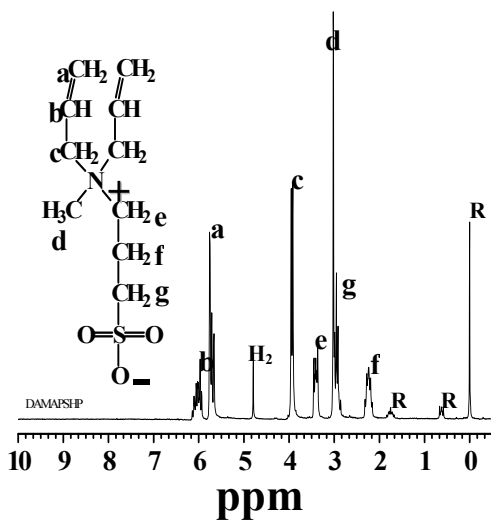


Figure 1. ^1H NMR spectrum 3-(N,N-diallyl-N-methyl ammonio) propane sulfonate (DAMAPS) in D_2O . R = 3-(trimethylsilyl)-1-propanesulfonic acid, sodium salt as a reference.

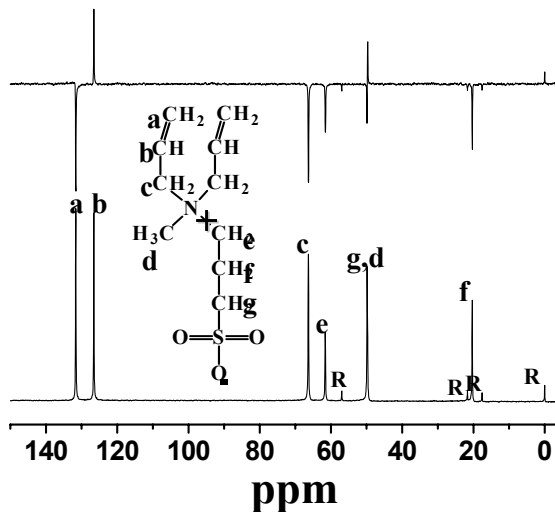
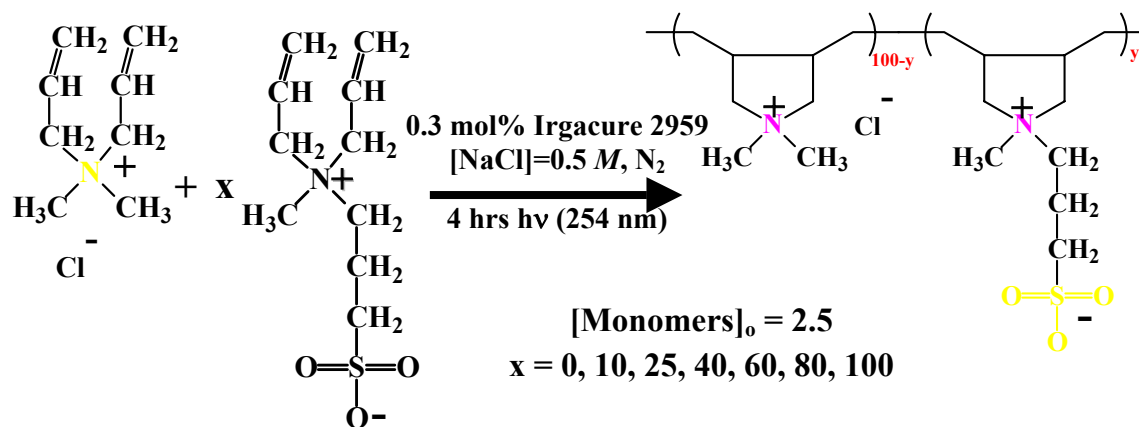


Figure 2. ^{13}C NMR and DEPT135 spectra of 3-(N,N-diallyl-N-methyl ammonio) propane sulfonate (DAMAPS) in D_2O . R = 3-(trimethylsilyl)-1-propanesulfonic acid, sodium salt as a reference.

Polymer Synthesis

Copolymers of DAMAPS with DADMAC (DADS)

The copolymerization of DADMAC with DAMAPS was conducted photochemically as depicted in Scheme 2. The water-soluble photoinitiator utilized was 2-hydroxy-1-[4-(hydroxyethoxy)phenyl]-2-methyl-1-propanone (Irgacure 2959). This initiator undergoes a Norrish Type I cleavage leading to the formation of the initiating species. This mechanism of photoinitiation was chosen since facile production of high concentrations of radicals occurs in short lengths of time, an attribute that is not typically observed in classical thermal polymerization of the diallyl ammonium salts. No phase separation or precipitation of the polymers occurred during polymerization, indicating homogeneous polymerization conditions persisted throughout the reaction.



Scheme 2. Synthetic pathway for preparation of DADMAC-co-DAMAPS cyclocopolymers.

Representative inverse gated decoupled ^{13}C NMR spectra are shown in Figure 3. Peak assignments were confirmed through DEPT135 analysis. (Data not shown.) The five-membered ring structure found in poly(DADMAC)⁶¹ was retained for each copolymer regardless of the incorporation of the sulfobetaine mer unit. Also, the *cis* conformation, which is the primary isomer found in the DADMAC homopolymer,⁶¹ was also confirmed in the sulfobetaine copolymers by analysis of the backbone carbon resonances at 28.8 and 40.7 ppm for the *cis* isomer and 32.6 and 45.7 ppm for the *trans* isomer, respectively.

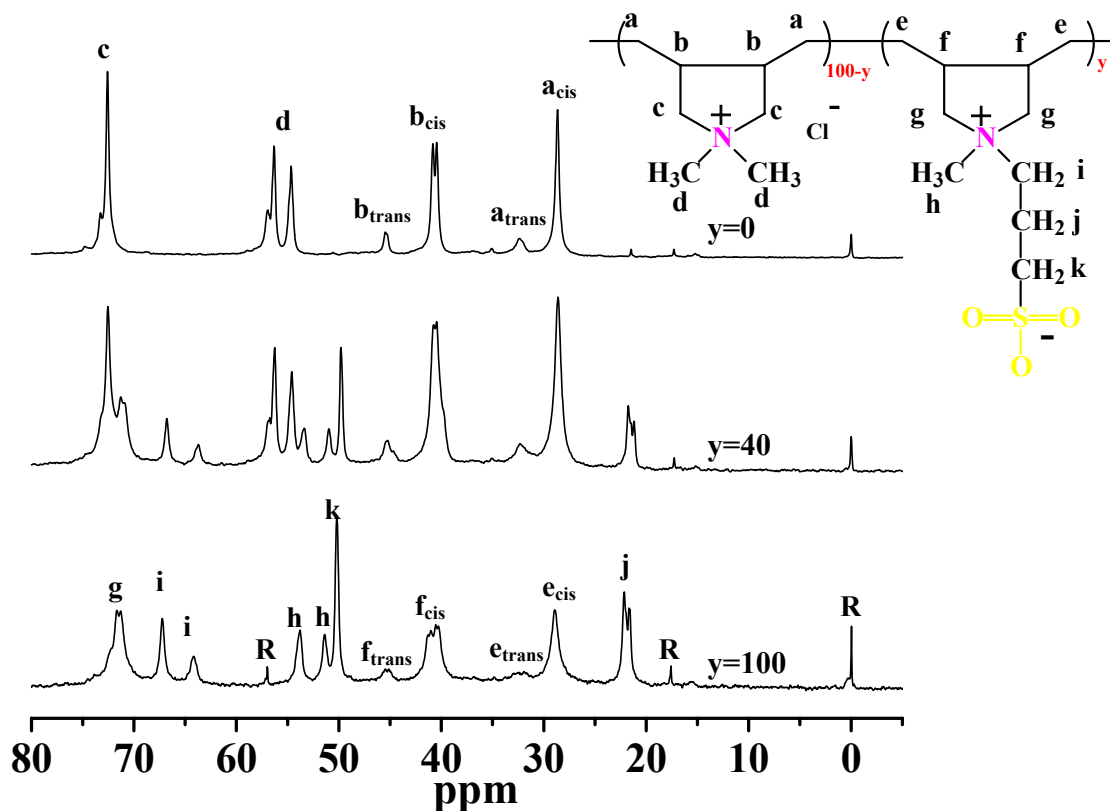
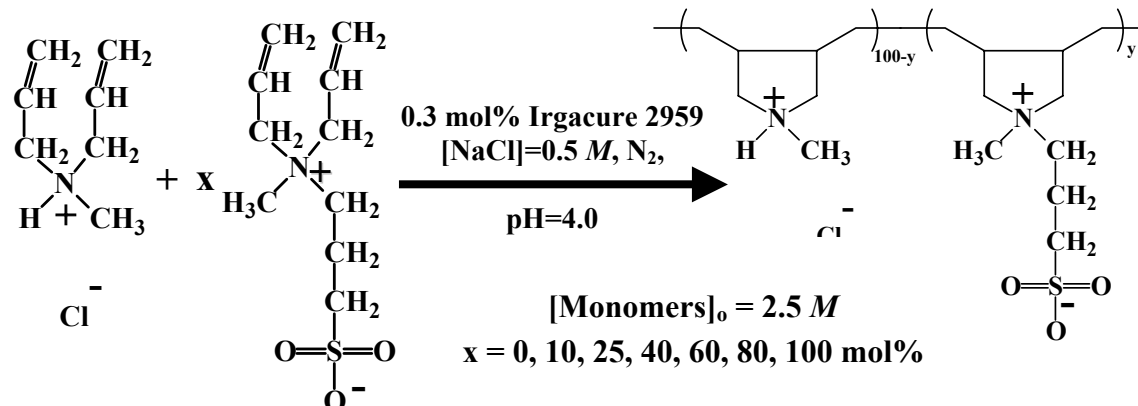


Figure 3. Representative inverse gated decoupled ^{13}C NMR spectra of the DADMAC-co-DAMAPS cyclocopolymers in D_2O (1M NaCl). (R = 3-(trimethylsilyl)-1-propanesulfonic acid, sodium salt as a reference.)

Copolymers of DAMA with DAMAPS (DAMS)

The copolymerization of DAMA with DAMAPS was conducted photochemically as shown in Scheme 3. The water-soluble photoinitiator, 2-hydroxy-1-[4-(hydroxy-ethoxy)phenyl]-2-methyl-1-propanone (Irgacure 2959), undergoes a Norrish Type I cleavage. This mechanism of photoinitiation results in rapid production of high concentrations of radicals, an attribute that is not typically observed in classical thermal polymerization of the diallyl ammonium salts. No phase separation or precipitation of the polymers occurred during polymerization, indicating that homogeneous polymerization conditions persisted throughout the reaction.



Scheme 3. Synthetic pathway for preparation of DAMA-co-DAMAPS cyclocopolymers

Representative inverse gated decoupled ¹³C NMR spectra are shown in Figure 4. Peak assignments were confirmed through DEPT135 analysis. The five-membered ring structure found in poly(DADMAC)⁶² was retained for each copolymer regardless of the incorporation of the sulfobetaine mer unit. Also, the *cis* conformation, which is the primary isomer found in the DADMAC homopolymer,⁶¹ was also confirmed to be the predominant isomer for this copolymer series by analysis of the backbone carbon resonances indicated in Figure 1.

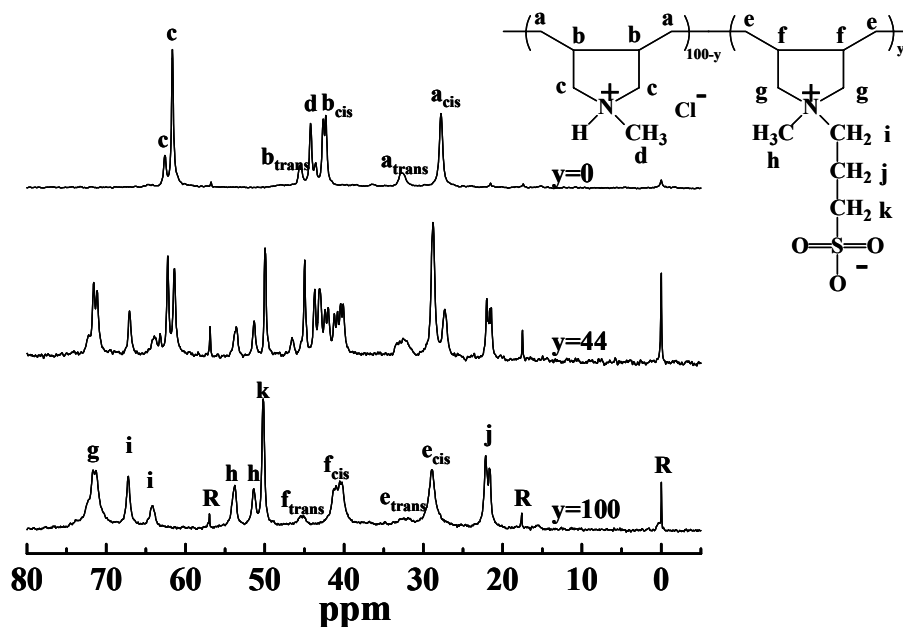


Figure 4. Representative inverse gated decoupled ¹³C NMR spectra of the DAMA-co-DAMAPS cyclocopolymers in D₂O (1M NaCl, pH=4.0). (R = 3-(trimethylsilyl)-1-propanesulfonic acid, sodium salt as a reference.)

Polymer Characterization

Compositional Analysis

Copolymer compositions for both systems were determined by the procedure introduced in the experimental section. From the experimentally-determined compositions of the low conversion samples, reactivity ratios of $r_1 = 1.14 \pm 0.05$ and $r_2 = 0.96 \pm 0.05$ for DADMAC(M_1)/DAMAPS(M_2) were determined by a nonlinear least squares method.⁶³ The experimentally measured values of copolymer composition as a function of feed compositions are shown in Figure 5; the dashed line represents ideal incorporation. Random (nearly ideal) incorporation was expected due to the identical polymerizable moieties present in DADMAC and DAMAPS. As a consequence of the nearly ideal copolymerization, the copolymers are characterized by significant chemical homogeneity, and the solution behavior should not be affected by microarchitectural differences in the copolymers. (Data summarized in Table 1)

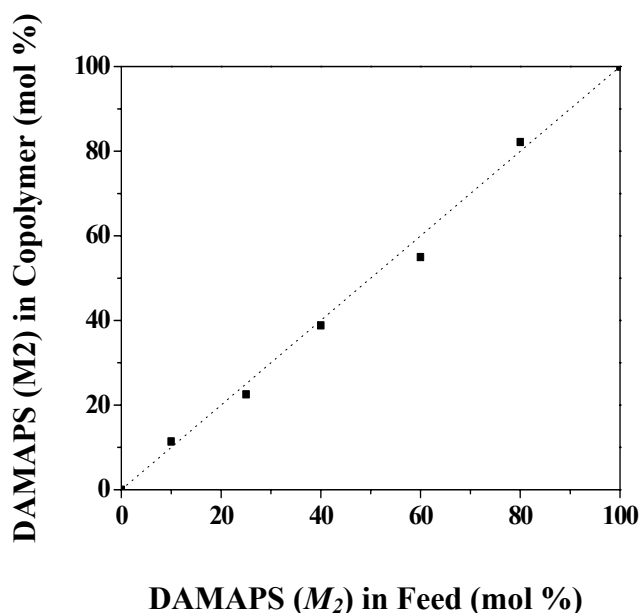


Figure 5. Mol% sulfobetaine incorporation as a function of mol % sulfobetaine in the feed as determined by inverse gated decoupled ^{13}C NMR.

Table 1. Reaction parameters and polymer composition for the copolymerization of DADMAC (M_1) and DAMAPS (M_2)

Sample	Rxn Time (hr)	% Conv.	M_2 Feed (mol%)	M_2 in copolymer (mol%) ^a	M_2 in <i>cis</i> Isomer (mol%) ^a
DADMAC	4.0	41	0	0 ^b	89
DADS11	4.0	35	10	11	90
DADS23	4.0	43	25	23	90
DADS40	4.0	40	40	40	89
DADS55	4.0	37	60	55	88
DADS82	4.0	38	80	82	89
DAMAPS	4.0	69	100	100 ^b	89

^a From inverse gated decoupled ¹³C NMR (D₂O) ^bTheoretical value

For the copolymer system of DAMA and DAMAPS, reactivity ratios of $r_1 = 0.67 \pm 0.05$ and $r_2 = 1.13 \pm 0.05$ for DAMA(M_1)/DAMAPS(M_2) were determined by a nonlinear least squares method.⁶⁴ (Data summarized in Table 2) The experimentally measured values of copolymer composition as a function of feed compositions are shown in Figure 6; the dashed line represents ideal incorporation. Random incorporation (with a slight tendency towards DAMAPS incorporation) was confirmed through microstructural composition analysis using the methods of Igarashi⁶⁵ with these reactivity ratios (Table 3).

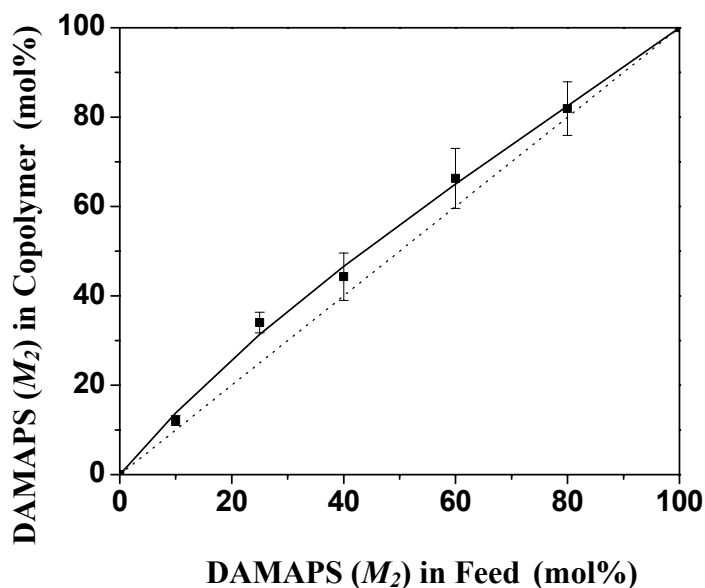


Figure 6. Mol% sulfobetaine incorporation in DAMA-co-DAMAPS copolymers as a function of mol% sulfobetaine in the feed as determined by inverse gated decoupled ¹³C NMR.

Table 2. Reaction parameters and polymer composition for the copolymerization of DAMA (M_1) and DAMAPS (M_2)

Sample	Rxn Time (hr)	% Conv.	M_2 Feed (mol %)	M_2 in copolymer (mol %) ^a	<i>cis</i> Isomer (mol %) ^a
DAMA	4.0	42.6	0	0 ^b	80
DAMS12	4.0	47.2	10	12	82
DAMS34	4.0	41.5	25	34	82
DAMS44	4.0	41.5	40	44	84
DAMS66	4.0	43.1	60	66	85
DAMS82	4.0	51.1	80	82	88
DAMAPS	4.0	69.0	100	100 ^b	89

^a From inverse gated-decoupled ¹³C NMR (1M NaCl, pH=4.0, D₂O). ^b Theoretical value.

Table 3. Microarchitectural Analysis: Distribution of Monads, Dyads and Triads per 100 Repeats as a Function of the Monomer Feed Ratio ($M_1:M_2$)

Sequence	90:10	75:25	60:40	40:60	20:80
M_1	86.2	68.6	53.4	35.0	17.5
M_2	13.8	31.4	46.6	65.0	82.5
M_1-M_1	73.9	45.8	26.8	10.8	2.51
M_1-M_2	12.3	22.8	26.6	4.18	15.0
M_2-M_1	12.3	22.8	26.6	4.18	15.0
M_2-M_2	1.53	8.56	20.0	40.8	67.5
$M_1-M_1-M_1$	63.4	30.6	13.4	3.33	0.36
$M_1-M_1-M_2$	10.5	15.2	13.4	7.47	2.15
$M_1-M_2-M_1$	10.9	16.6	15.2	8.99	0.72
$M_1-M_2-M_2$	1.36	6.22	11.7	15.2	12.3
$M_2-M_1-M_1$	10.5	15.2	13.4	7.47	2.15
$M_2-M_1-M_2$	1.74	7.58	13.3	16.7	12.8
$M_2-M_2-M_1$	1.36	6.22	11.4	15.2	12.3
$M_2-M_2-M_2$	0.17	2.34	8.57	25.7	55.3

Light Scattering Analysis

Weight-average molecular weights were determined by Berry Plots at 25°C in 1 M NaCl. For the DAMS series, a pH of 4 was maintained. The data can be seen in Tables 4 and 5. Molecular weight values might seem low for free radical polymerizations, but these are typical for diallyl ammonium salt monomers. The likely reason for moderate molecular weight polymers is chain transfer to monomer involving the labile allylic hydrogen atoms.

Table 4. Classical light scattering data for the copolymers of DADMAC (M_1) with DAMAPS (M_2) in 1 M NaCl.

Sample	M_2 in copolymer (mol%) ^a	dn/dc (ml/g)	$M_w \times 10^{-4}$ (g mol ⁻¹)	$A_2 \times 10^4$ (ml mol g ⁻²)	$DP_w \times 10^{-2}$
DADMAC	0 ^b	0.171±0.003	5.16	5.54	3.2
DADS11	11	0.168±0.003	5.97	4.75	3.6
DADS23	23	0.173±0.001	6.51	3.90	3.6
DADS40	40	0.157±0.003	7.28	2.24	3.8
DADS55	55	0.158±0.001	7.22	1.89	3.5
DADS82	82	0.157±0.001	7.87	2.07	3.6
DADS100	100 ^b	0.153±0.001	8.42	2.14	3.6

^a From inverse gated-decoupled ¹³C NMR (D₂O) ^b Theoretical value

Table 5. Classical light scattering data for the copolymers of DAMA (M_1) with DAMAPS (M_2).

Sample	M_2 in copolymer (mol%) ^a	$M_w \times 10^{-4}$ (g mol ⁻¹)	$A_2 \times 10^4$ (ml mol g ⁻²)	$DP \times 10^{-2}$
DAMA	0 ^b	4.13	2.19	2.80
DAMS12	12	4.00	4.62	2.28
DAMS34	34	5.36	3.75	2.36
DAMS44	44	4.32	2.85	1.72
DAMS66	66	5.81	2.42	1.93
DAMS82	82	6.83	2.29	2.02
DAMAPS	100 ^b	8.42	2.14	3.61

^a From inverse gated-decoupled ¹³C NMR (1M NaCl, pH=4.0, D₂O) ^b Theoretical value

It is important to note that for the DADS copolymer systems, the range of the degree of polymerization for this copolymer series remains narrow (3.2-3.8)×10² for otherwise identical copolymerization conditions. Therefore, the kinetic chain length appears quasi-independent of the monomer feed ratio, a feature which is in good agreement with $r_1 \sim r_2 \sim 1$ and provides further support for the identical polymerization behavior of the two monomers. Also, since the values obtained for the DP_w for each copolymer are similar, any differences in solution properties are a result of changes in chemical composition, and not due to the length of the copolymer chain.

Polymer Solution Behavior of DADS Copolymer Series

Effects of Copolymer Composition and added Salt

During initial solubility experiments, it was discovered that copolymers containing ≤55 mol% of the sulfobetaine moiety were soluble in deionized water, a characteristic not commonly attributed to polysulfobetaines. In this case, the charge-charge repulsion of the excess positive charges along the polymer backbone (DADMAC mer units) allows the polymer to assume an expanded conformation in deionized water. This is illustrated in Figure 7, which shows the

reduced viscosity of the DADS series in deionized water as a function of polymer concentration. It may be seen from Figure 7 that the DADS series exhibits classical polyelectrolyte solution behavior; in that the reduced viscosity increases dramatically as the polymer concentration decreases. However, the magnitude of the response diminishes with increased incorporation of the sulfobetaine mer units due to the replacement of an ionic charge with a dipole. It is likely that chain collapse occurs due to dipole-dipole intramolecular interactions between sulfobetaine moieties. (μ of the zwitterionic moiety has been determined to be 23.0 D for triethylammoniopropanesulfonate.⁶⁶) Also, it should be noted that the reduced viscosity decreases as the incorporation of the sulfobetaine moiety increases, again from the intramolecular aggregation brought about by dipole-dipole interactions.¹³ This collapse is also observed in light scattering by a decrease in the polymer-solvent interaction parameter, A_2 , as the mol % sulfobetaine increases (Table 4).

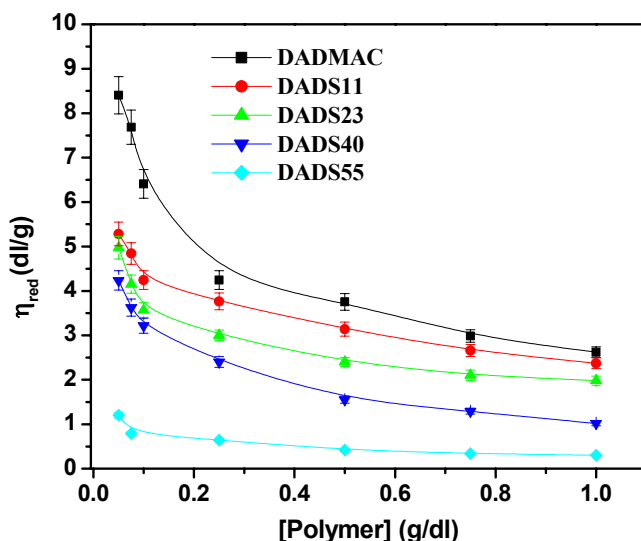


Figure 7. Reduced viscosity as a function of polymer concentration for the homopolymer of DADMAC and copolymers of DADMAC and DAMAPS in deionized water ($T = 25^\circ\text{C}$, $\gamma = 5.96 \text{ s}^{-1}$).

The aqueous solution properties of this copolymer series were further evaluated by observing apparent viscosity changes with increasing polymer concentration and ionic strength (Figure 8). Data for the homopolymer of DADMAC and three copolymers of DADMAC and DAMAPS are plotted. The apparent viscosities of the polymer solutions decrease as the molar incorporation of the sulfobetaine moiety increases for selected values of ionic strength. Also, as the ionic strength of the aqueous medium is increased, the apparent viscosity of each polymer solution decreases, a characteristic common to polyelectrolytes. However, for copolymers with higher incorporations of the sulfobetaine, an increase in the apparent viscosity at elevated NaCl concentrations is observed. Evidently, the initial decrease in apparent viscosity is due to the shielding of the charge-charge repulsions along the polymer backbone. When these repulsive

forces are diminished, the dipole-dipole interactions allow the copolymer to assume a collapsed conformation, which is manifested by a minimum in the apparent viscosity. As the ionic strength of the medium is increased further, the dipole-dipole interactions are minimized, and chain expansion occurs. The increase in apparent viscosity is better visualized by replotting the data on a smaller scale as depicted in Figure 9.

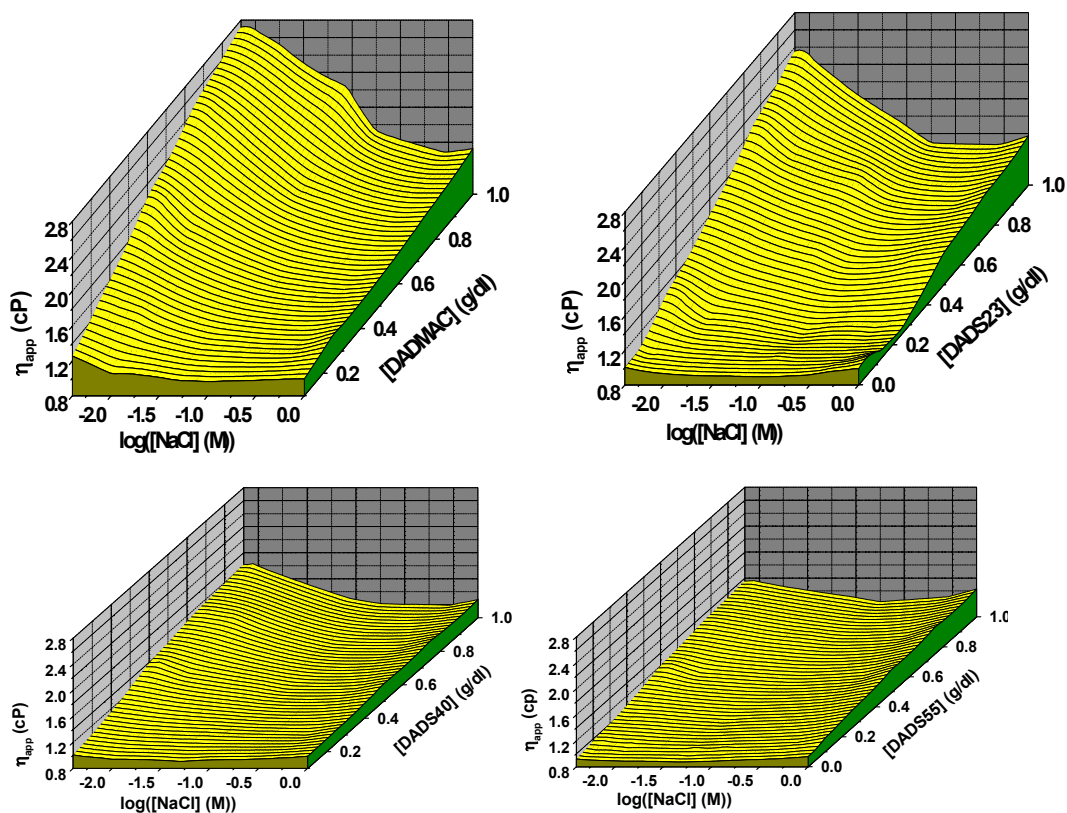


Figure 8. Apparent viscosity for the homopolymer of DADMAC and three copolymers of DADMAC and DAMAPS as functions of NaCl and polymer concentrations ($T = 25^{\circ}\text{C}$, $\gamma = 5.96 \text{ s}^{-1}$).

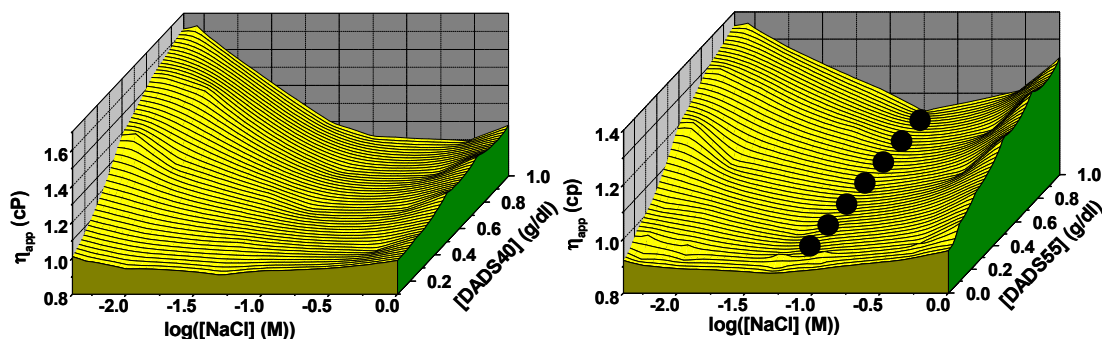


Figure 9. Apparent viscosity for DADS40 and DADS55 as functions of NaCl and polymer concentrations ($T = 25^{\circ}\text{C}$, $\gamma = 5.96 \text{ s}^{-1}$) (● Represents regions of macroscopic phase separation.)

It must be pointed out that for DADS55 at $0.075 \text{ M} < [\text{NaCl}] < 0.5 \text{ M}$, the dipole-dipole associations are sufficiently prevalent to bring about macroscopic phase separation. Figure 10 clearly illustrates the presence of polymer-rich and polymer-poor phases at $[\text{NaCl}] = 0.1$ and 0.5 M . Above and below this critical concentration range, a macroscopically homogeneous solution is observed.

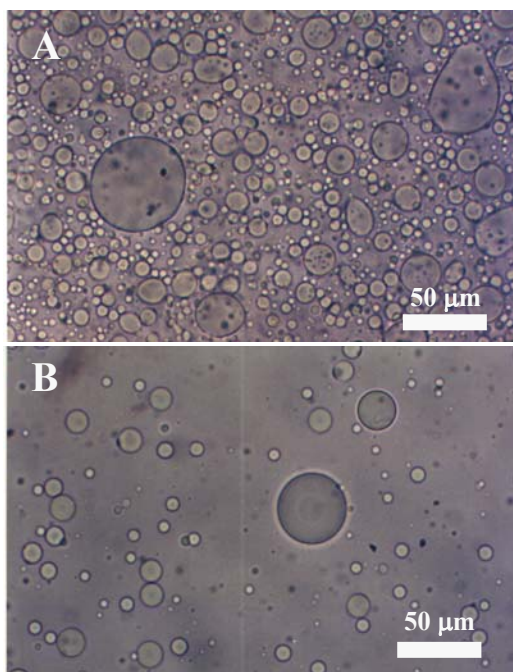


Figure 10. Optical micrographs of aqueous solutions of DADS55 in (A) 0.1 M and (B) 0.5 M NaCl ($T = 25^{\circ}\text{C}$, $[\text{DADS55}] = 1.0 \text{ g/dl}$).

In order to study the above macroscopic events observed on the molecular level, dynamic light scattering experiments were performed on the DADS40 copolymer as a function of NaCl and polymer concentrations. DADS40 is especially interesting since it maintains macroscopic homogeneity throughout the NaCl and polymer concentration ranges studied and exhibits a large increase in viscosity at elevated NaCl concentrations. Figure 11 is a three-dimensional plot of the hydrodynamic radius of the DADS40 copolymer as functions of NaCl and polymer concentrations. As can be discerned from the figure, for any given polymer concentration, as the ionic strength of the medium is increased, the hydrodynamic radius initially decreases, reaches a minimum, and then increases. This correlates directly with the apparent viscosity data illustrated in Figure 8.

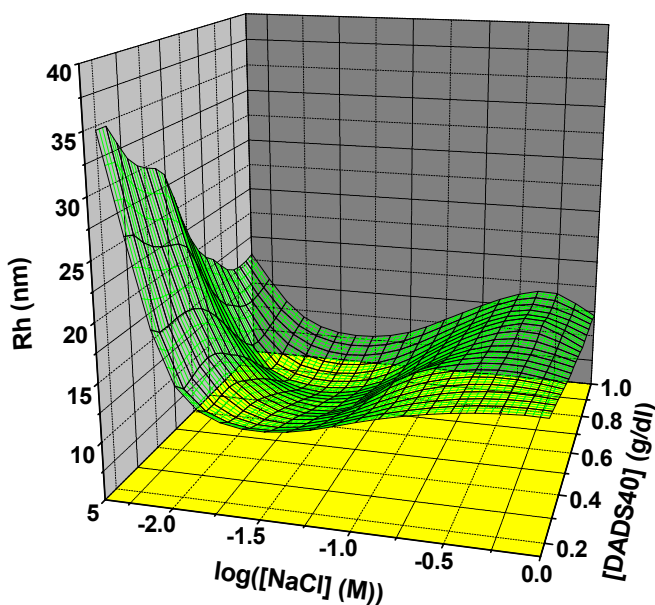


Figure 11. Hydrodynamic radius of DADS40 as functions of NaCl and polymer concentrations (T = 25°C).

Based upon the low-shear viscosity and dynamic light scattering data, an association model for the copolymers of DADMAC and DAMAPS as a function of NaCl concentration is presented in Figure 12. For copolymers with a low molar incorporation of the sulfobetaine moiety, classical polyelectrolyte behavior is observed. As the ionic strength of the medium is increased, the small molecule electrolyte counter-ions shield the backbone cationic repulsions, allowing the polymer to assume a more random conformation. For copolymers containing 40-55

mol% DAMAPS, the polymer chain assumes a compact conformation due to intramolecular dipole-dipole interactions. However, a sufficient number of excess positive charges along the copolymer backbone, allow solubility. As the ionic strength is further increased, the charge-charge repulsion of the excess positive charge is diminished and a further collapse of the polymer chain is realized. (This collapse leads to macroscopic phase separation of the DADS55 copolymer.) As the ionic strength is increased further, the dipole-dipole interactions of the sulfobetaine mer units are diminished allowing an expansion of the polymer coil.

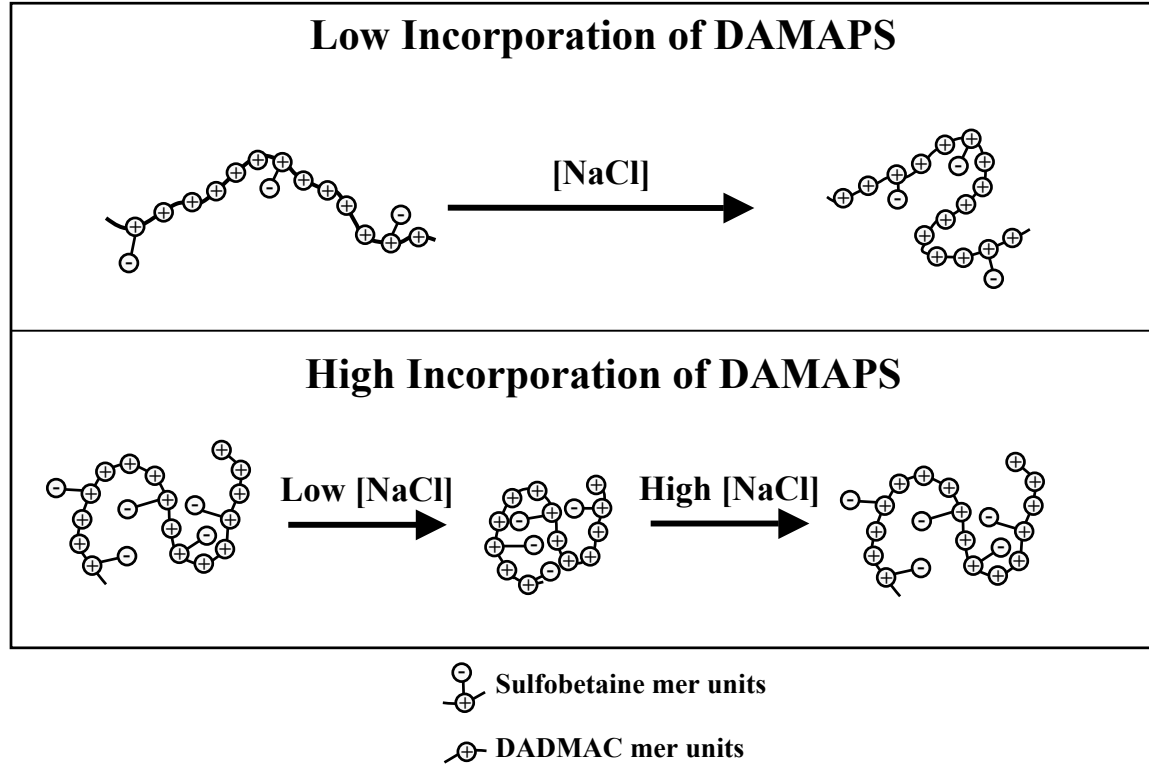


Figure 12. Proposed polymer conformational changes for copolymers of DADMAC and DAMAPS as a function of NaCl concentration.

The above model is consistent with recent theoretical efforts devoted to understanding the conformations of linear polyampholyte chains.⁶⁶⁻⁷⁰ For a polyampholyte with excess positive or cationic charge, the electrostatic interactions can be characterized by an excluded volume:

$$\nu^* = -\frac{\pi(fl_B)^2}{\kappa_s} + \frac{4\pi l_B \Delta f^2}{\kappa_s^2} \quad (5)$$

where l_B is the Bjerrum length, f is the total fraction of charged monomers, and κ_s is the usual Debye-Hückel screening parameter. The first term of eq. 5 describes the screening of attractive polyampholyte interactions and the second term describes the screening of repulsive interactions between excess charges. The electrostatic excluded volume is positive at low ionic strength, inducing a stretching of the chain. As the ionic strength is increased, the screening of Coulombic

repulsions is stronger than the screening of the polyampholyte attractions and the excluded volume becomes negative, thus inducing chain collapse. As the ionic strength is increased, the chain swells again because of the screening of the attractive polyampholyte interactions.

Polymer Solution Behavior of DAMS Copolymer System

Potentiometric and Turbidimetric Measurements

The aqueous solution behavior of the DAMS copolymer series was initially studied by performing potentiometric and turbidimetric titrations to determine the phase behavior as a function of the degree of ionization of the DAMA mer unit (α). Figure 13 illustrates the % Transmittance and apparent pK_a as a function of the degree of ionization of the DAMA mer unit (α) for the homopolymer (DAMA) and three copolymers of DAMA and DAMAPS (DAMS11, DAMS44, and DAMS66). The apparent pK_a was calculated utilizing the Henderson-Hasselbalch equation⁷¹:

$$pK_a = pH - \log \frac{\alpha}{1 - \alpha} \quad (6)$$

As shown in Figure 13, each of the polymers is soluble at high degrees of DAMA mer unit ionization. In this case, the polymers resemble copolymers of N,N-diallyl-N,N-dimethyl ammonium chloride (DADMAC) and DAMAPS which have been previously studied in our laboratories.⁷² In those studies, it was discovered that DADMAC-co-DAMAPS copolymers containing less than 55 mol % of the sulfobetaine mer unit exhibit solubility in deionized water due to a charge imbalance along the polymer backbone. The DAMA-co-DAMAPS copolymers also exhibit this behavior when the DAMA mer unit is protonated. However, as the degree of ionization decreases, the turbidity of the solution increases for DAMA, DAMS12, and DAMS66. In the case of the homopolymer, DAMA, the polymer precipitates from solution for $\alpha < 0.1$. Apparently, at low degrees of ionization, the hydrophobic tertiary amine functionality dominates the phase behavior and precipitation of the polymer results. DAMS12 does not precipitate from solution; however, macroscopic phase separation is observed for $\alpha < 0.1$. In this case, the incorporation of the hydrophilic sulfobetaine mer units help to stabilize the hydrophobic segments of the copolymer, but the molar content of the hydrophilic segment is not large enough to maintain solubility. DAMS34 (data not shown) and DAMS44, on the other hand, remain soluble throughout the entire range of α , due to sufficient hydrophilic content. However, as the sulfobetaine content increases to 66 mol% (DAMS66), macroscopic phase separation (but no precipitation) is again observed for low degrees of ionization of the DAMA mer unit ($\alpha < 0.2$). Instead of hydrophobic interactions dictating the phase separation, as in the case for DAMA and DAMS12, the likely molecular interactions dictating the phase behavior are the dipole-dipole interactions among the sulfobetaine mer units.

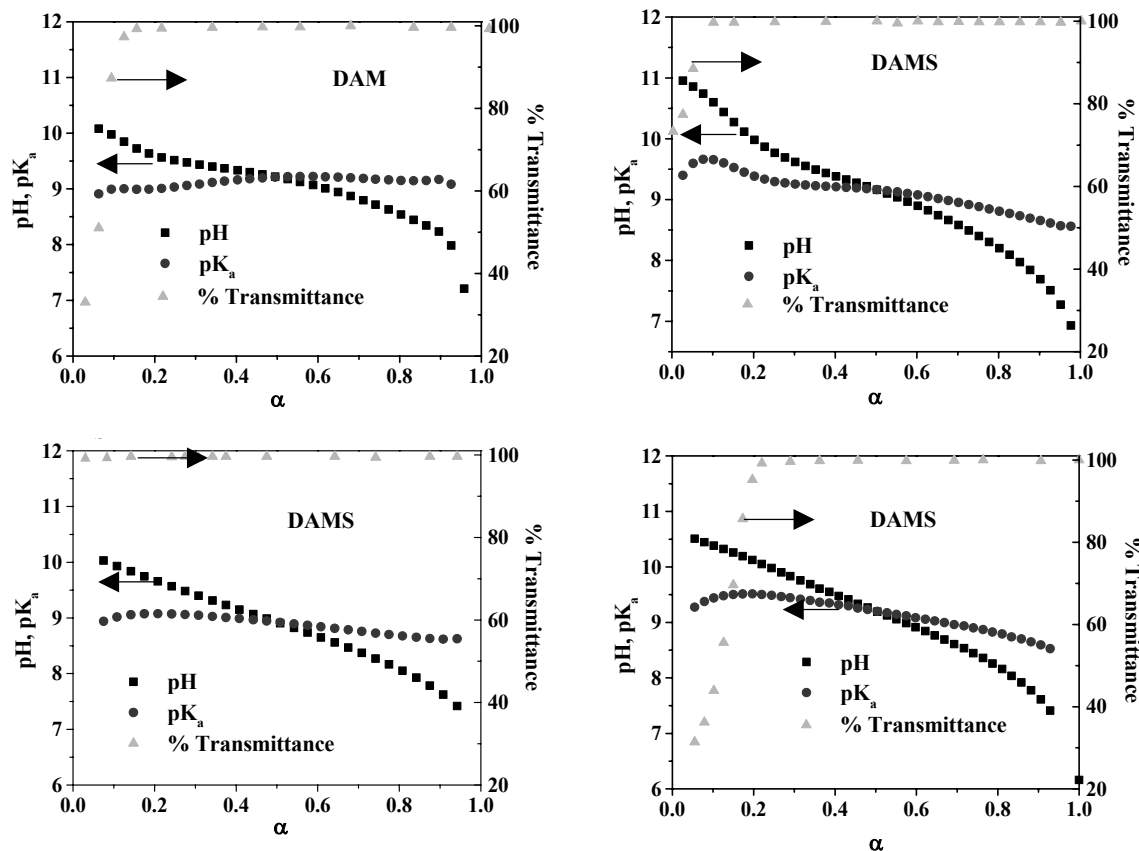


Figure 13. Potentiometric and turbidimetric titrations of DAMA and three copolymers of DAMA and DAMAPS (α represents the degree of ionization of the DAMA mer unit).

Viscometric Studies

In order to further study the solution behavior of the DAMA-co-DAMAPS polymer series, low-shear viscosity experiments were performed. Figure 4 illustrates the apparent viscosity for the homopolymer, DAMA, and three copolymers of DAMA and DAMAPS (DAMS34, DAMS44, and DAMS66) as functions of the degree of ionization of the DAMA mer unit (α) and polymer concentration. Note that for each system, the apparent viscosity of the polymer solution diminishes as α decreases. This behavior has been well documented as a polyelectrolyte-to-polysoap transition common to many responsive systems. At high α , the polymer assumes a more extended conformation due

to the charge-charge repulsive forces along the polymer backbone. However, as the degree of ionization is lowered, the mer unit that was once charged is transformed into a hydrophobic species, thus causing the polymer to assume a collapsed conformation.

Upon further analysis of Figure 14, one may determine the effects of the incorporation of the sulfobetaine mer unit on the conformation of the polymer chain in solution. Note that at high degrees of ionization of the DAMA mer unit, the apparent viscosity of the polymer systems decrease as the sulfobetaine incorporation increases, a characteristic similar to that exhibited by

DADMAC-*co*-DAMAPS copolymers.⁷² The decrease in apparent viscosity is attributed to an increase of intramolecular dipole-dipole interactions among the zwitterionic moieties. These interactions lead to a decrease in coil dimensions and thus a decrease in the viscosity of the system.

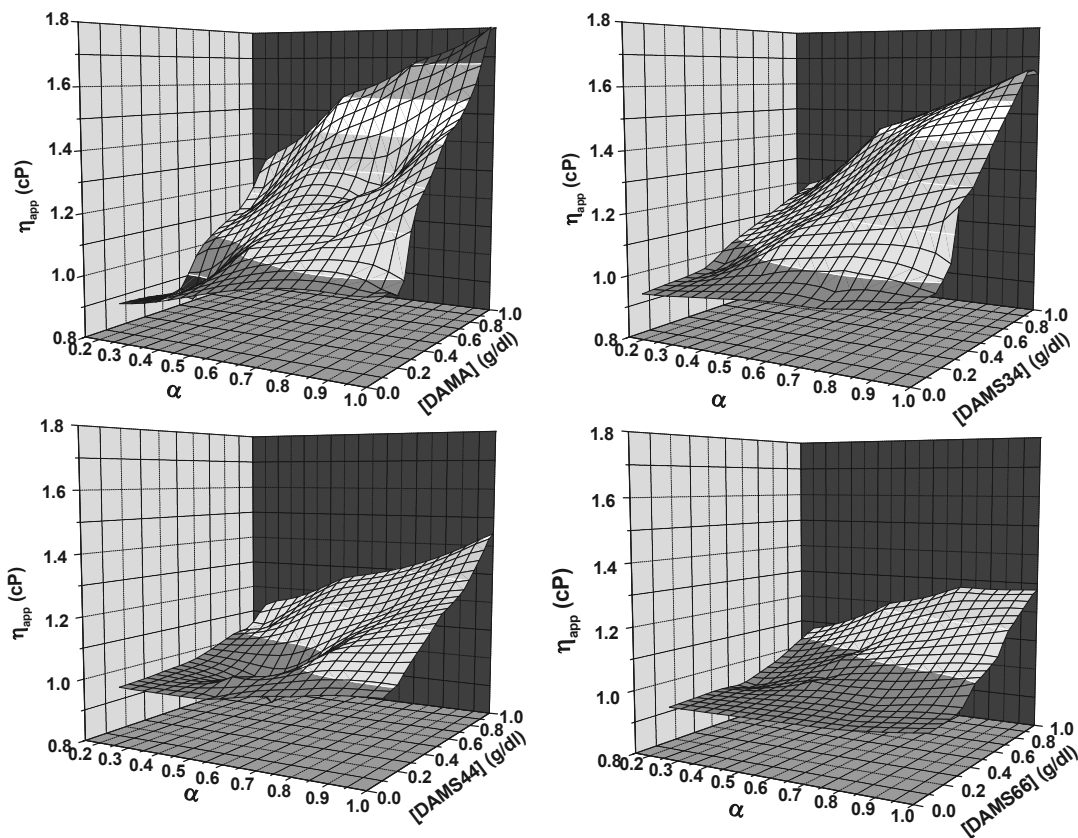


Figure 14. Apparent viscosity for the homopolymer of DAMA and three copolymers of DAMA and DAMAPS as functions of polymer concentration and the degree of ionization of the DAMA mer unit (α) ($T = 25^\circ\text{C}$, $\gamma = 5.96\text{s}^{-1}$).

For low degrees of ionization of the DAMA mer unit, the copolymers assume a collapsed conformation as discussed above. However, for dilute solutions, as the molar incorporation of the sulfobetaine mer units is increased from 0 to 44 mol%, the apparent viscosity increases. This is followed by a decrease in the apparent viscosity as the molar incorporation reaches 66 mol %. The sulfobetaine mer units act as a hydrophilic segment, and thus stabilizes the polymer in solution and hinders the total collapse of the polymer chain. However, if the molar incorporation of the sulfobetaine unit is increased above 44 mol % it appears that the dipole-dipole interactions begin to dominate the solution behavior as demonstrated by a decrease in viscosity and ultimate phase separation for $\alpha < 0.1$.

Since the viscosity experiments indicate that a polyelectrolyte-to-polysoap transition is occurring as a function of the degree of ionization of the DAMA mer unit (by changes in pH), equilibrium surface tension measurements were performed to monitor the packing of the polymer chains at an air-water interface. Figure 15 illustrates the equilibrium surface tension for DAMA and DAMS44 as a function of polymer concentration at specific pH values. As can be clearly seen from the figure, DAMA exhibits pH-responsive surface activity. At high degrees of ionization, the charge-charge repulsions along the polymer backbone hinder hydrophobic association and thus hinder packing along the air-water interface. However, as the degree of ionization is decreased, the hydrophobic content of the homopolymer increases and packing at the surface is favored, thus causing the surface tension to decrease dramatically to an equilibrium value of ~ 32 mN/m². For DAMS44, surface activity is observed only at very low degrees of ionization of the DAMA mer unit. Still, even at pH 9.73 an equilibrium surface tension of ~ 55 mN/m² is measured. Once again the sulfobetaine mer unit is sufficiently hydrophilic to hinder the hydrophobic collapse of the polymer chain and packing at the air-water interface.

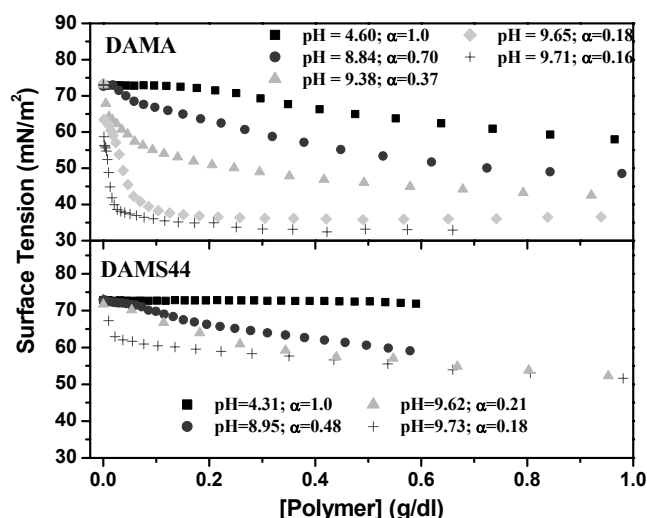


Figure 15. Equilibrium surface tension for DAMA and DAMS44 polymers as a function of polymer concentration at selected degrees of ionization of the DAMA mer units (α) ($T=25^{\circ}\text{C}$).

Equilibrium Dialysis/Sequestration Studies

The pH-responsive surface activity of the DAMA-co-DAMAPS copolymers suggests application in micellar enhanced ultrafiltration for the removal of organic foulants from wastewater streams. In order to investigate the pH-controlled solubilization of a model organic solute (*p*-cresol), equilibrium dialysis experiments were performed utilizing DAMA and DAMS44 at various pH conditions. Equilibrium dialysis experiments were selected since they are often utilized to mimic micellar enhanced ultrafiltration processes.⁶⁰ For these investigations, the polymer concentration was held constant at 0.2 g/dl, since at this concentration the polymers exhibit no surface activity at high α , and a maximum surface activity at low α .

The binding isotherms and the corresponding hydrodynamic diameters of the polymer-foulant complexes for DAMA and DAMS44 are illustrated in Figures 16 and 17, respectively. Based on the surface tension and viscometric data, which indicates that the DAMA homopolymer assumes an expanded conformation at high degrees of ionization, one would not expect to observe sequestration of *p*-cresol by the polymer. Figure 16 confirms this assumption by indicating minimal binding of the organic solute below a critical *p*-cresol concentration. However, at high concentrations of *p*-cresol, the model foulant induces intermolecular aggregation of the homopolymer and binding is observed. (Even at $\alpha=1.0$, the homopolymer contains a hydrophobic group at the chain end arising from the initiating species.) Transition to the aggregated form is readily detected through dynamic light scattering experiments which indicate the formation of large aggregates of ~ 150 nm and ~ 200 nm for $\alpha=1.0$ and $\alpha=0.94$, respectively. (It must be pointed out that the molecular dimensions of the DAMA homopolymer (with no binding of *p*-cresol) could not be determined due to the appearance of a slow mode of relaxation common to polyelectrolytes.⁷³⁻⁷⁵) As the degree of ionization of the DAMA homopolymer decreases, the polymer becomes more hydrophobic and binding of *p*-cresol increases dramatically as indicated in the binding isotherm. The polymer binds such a large quantity of *p*-cresol that large macromolecular structures are formed, resulting in solution turbidity which precluded the determination of the molecular dimensions of the multi-chain/*p*-cresol complexes by dynamic light scattering.

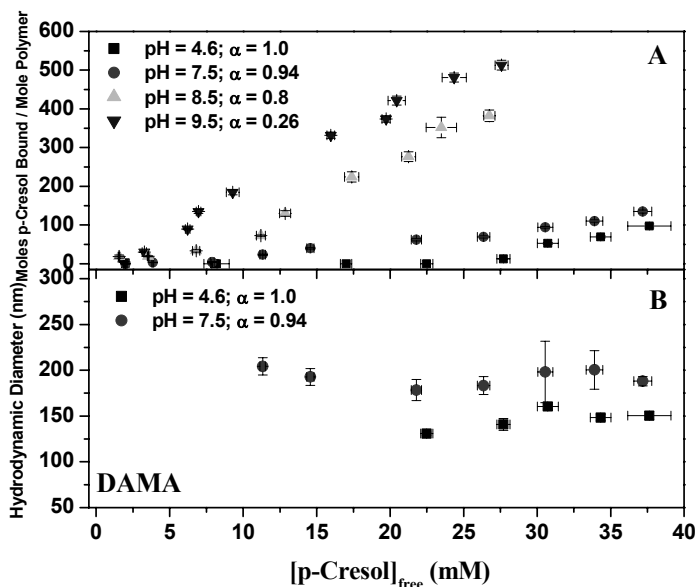


Figure 16. Binding isotherms for DAMA and *p*-cresol (A) and the corresponding hydrodynamic diameter of the polymer-foulant complex (B) as a function of *p*-cresol concentration and the degree of ionization of the DAMA mer unit (α) ($[DAMA]=0.2$ g/dl; $T=25^{\circ}\text{C}$).

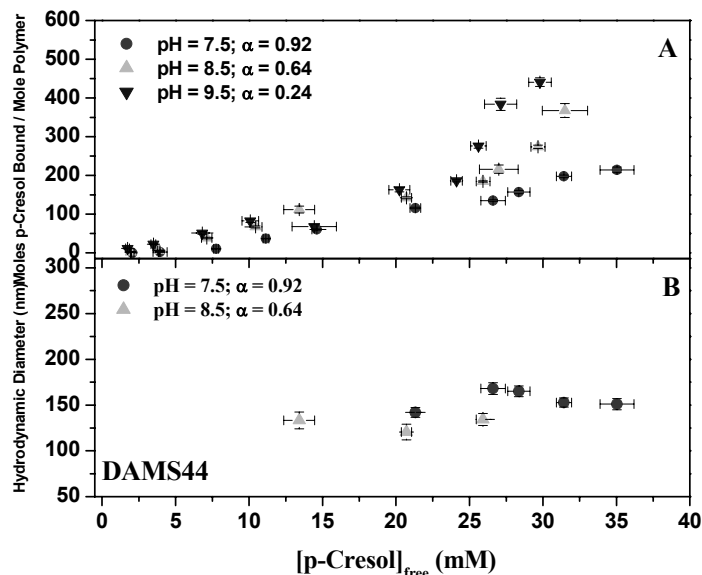


Figure 17. Binding isotherms for DAMS44 and *p*-cresol (A) and the corresponding hydrodynamic diameter of the polymer-foulant complex (B) as a function of *p*-cresol concentration and the degree of ionization of the DAMA mer unit (α) ([DAMS44]=0.2 g/dl; T=25°C).

In closely analyzing the binding of *p*-cresol to DAMS44, several differences from the data obtained for the DAMA homopolymer are observed. At high degrees of ionization, it appears that the DAMS44 copolymer solubilizes slightly more *p*-cresol than the DAMA homopolymer. From the viscometric data at $\alpha \sim 1$, it was determined dipole-dipole interactions among sulfobetaine mer units cause the polymer chain to assume a more collapsed conformation than the DAMA homopolymer. This relaxed conformation appears to facilitate the sequestration of the organic solute. As the degree of ionization decreases, solubilization of *p*-cresol by DAMS44 increases due to the formation of larger hydrophobic segments along the polymer backbone. However, the amount of the organic solute sequestered within the hydrophobic domains is much less than that of the DAMA homopolymer. This is not unexpected based on the surface tension and viscosity data, which indicate that the incorporation of the sulfobetaine hinders packing of the hydrophobic moieties, and therefore hinders sequestration of the organic solute.

Once again, determination of the size of the polymer/foulant complex is complicated due to the appearance of the slow mode of relaxation for samples at high degrees of ionization and the turbidity developed at high concentrations of *p*-cresol and lower degrees of ionization. However, despite these complications, it is apparent from the molecular dimensions determined from dynamic light scattering that the complexes formed are comprised of multiple polymer chains.

In order to evaluate utility in a micellar enhanced ultrafiltration application, rejection ratios were calculated for each copolymer under various environmental conditions (Table 4). Rejection ratios indicate the percentage of the small molecular solute retained within a hydrophobic domain. As can be seen by analysis of Table 6, the maximum rejection ratio obtained under this study is ~60 %. Although, this value might seem low for ultimate utility in an ultrafiltration application, (rejection ratios for 1-hexadecylpyridinium chloride/*p*-cresol complexes are often >97 %),⁷⁶ the efficiency of DAMA-based copolymer systems may be increased with a multiple-pass configuration. In addition, the DAMA-based copolymers offer other advantages over conventional surfactants in MEUF applications. These polymeric systems are quantitatively retained by the filtration membrane and pose no threat as a potential pollutant in the clean water (permeate) stream (a common problem in MEUF applications as discussed above). Also, as evidenced by the dynamic light scattering data, the molecular dimensions of the polymer/foulant complex are much larger than the surfactant/foulant complexes found in typical micellar enhanced ultrafiltration. Due to the larger size of the aggregates, membranes with larger pore sizes may be selected, therefore increasing the permeate flux. In addition, due to the pH-responsive behavior of the DAMA-based copolymers, the polymer/foulant complex may be broken by changes in pH, thus providing a facile mechanism of foulant removal from sequestering domains.

Table 6. Rejection Ratios as a function of [Cresol]_{feed}, and pH for DAMA and DAMS44.

[Cresol] _{feed} (mM)	DAMA pH=4.6	DAMA pH=7.5	DAMA pH=8.5	DAMA pH=9.4	DAMS44 pH=7.5	DAMS44 pH=8.5	DAMS44 pH=9.5
4	<1%	<1%	36±8%	12±1%	<1%	4.5±0.2%	23±2%
8	<1	<1%	21±1	31±3	2.7±0.3	6.9±0.1	22±1
16	<1	<1%	26±2	36±2	5.8±0.1	20±1	25±2
24	<1	2±1	24±1	59±3	13±1	23±1	27±2
32	<1	4±1	33±2	59±5	16±1	28±2	26±2
48	<1	5±1	43±2	50±2	20±2	24±1	27±1
56	2±1	6±1	39±2	45±6	19±1	22±1	28±1
64	8±1	8±1	42±3	53±3	20±2	27±1	33±1
72	9±1	11±1	41±2	49±2	22±2	30±1	39±2
80	11±1	13±1	41±2	47±2	22±2	35±2	40±1

Conclusions

A sulfobetaine monomer, 3-(*N,N*-diallyl-*N*-methyl ammonio) propane sulfonate, has been synthesized and copolymerized with *N,N*-diallyl-*N,N*-dimethylammonium chloride and *N,N*-diallyl-*N*-methyl amine. ¹³C NMR analysis indicates that the resulting polymers maintain the five-membered ring structure common to cyclopolymerized diallylammonium salts. The solution behavior of the DADS series is dictated by two opposing forces: cationic charge-charge repulsion along the polymer backbone from DADMAC mer units, and the dipole-dipole

attractive forces created by the presence of the sulfobetaine DAMAPS unit. Stimuli-responsive behavior including phase separation can be realized by adjusting ionic strength.

For the DADS series, reactivity ratio studies indicate random incorporation of the two mer units with a slight tendency towards favored incorporation of the sulfobetaine. Turbidimetric titration, low-shear viscosity, and equilibrium surface tension experiments were utilized to study the solution behavior of the resulting copolymers. A proposed model of association is depicted in Figure 12. At high degrees of ionization, the copolymers assume an expanded conformation due to the charge-charge repulsions along the copolymer backbone. As the molar incorporation of the sulfobetaine increases (at high degrees of ionization), the copolymer assumes a more relaxed conformation due to dipole-dipole interactions. As the degree of ionization of the tertiary amine decreases, hydrophobic associations dominate the solution behavior. For copolymers with low incorporation of sulfobetaine, chain collapse leading to precipitation occurs. However, at higher incorporations, the sulfobetaine acts as a hydrophilic segment to limit hydrophobic packing and minimizes the chain collapse.

Equilibrium dialysis experiments have demonstrated that the DAMA-based copolymers may be utilized in a micellar-enhanced ultrafiltration application. A facile mechanism of foulant capture and release is provided by the pH-reversible domains.

Task 5: Polymer Solution Mobility Studies

Introduction

Polymer solutions used in enhanced oil recovery (EOR) experience environmental changes when pumped into underground reservoirs. Structural characteristics of the polymer molecules can cause variations in polymer coil conformation as the solution environment changes, leading to changes in solution properties (i.e. viscosity). These changes in solution viscosity can enhance or degrade oil displacement efficiency during reservoir flooding. Thus, an understanding of how polymer solution viscosities change is important to EOR.

Solution conditions are multivariable and extensive experimentation is often necessary to map polymer solution behavior over the range of conditions encountered in EOR. In an effort to reduce experimentation, we have worked toward the development of a theoretical model to describe polymer solution behavior as a function of its solution environment. Ideally, with a good model defined, fewer experiments will be needed because one or two physical parameters unique to the polymer-solvent system can predict solution properties at the conditions in question.

Previously, we developed and provided justification for a thermodynamic theory that describes polymer solution intrinsic viscosity as a function of weight average polymer molecular weight and solution temperature.⁷⁷ In our last report⁷⁸ we developed a modification of the Odjik, Skolnick, Fixman (OSF) theory to account for intrinsic viscosity increases due to electrostatic repulsions between charges on polyelectrolytes. We fit the model to data found in the open literature for several different polymers over ranges of solution ionic strength and polymer charge distribution. An apparent universal relationship was reported describing polyelectrolyte solution intrinsic viscosity as a function of the ratio of the Debye-Hückel screening length (a function of solution salt concentration) to the spacing between polyelectrolyte charges.

While repulsive forces between similar charges tend to increase the intrinsic viscosity of polyelectrolytes, polyampholytes experience intramolecular attractions between oppositely charged constituents causing decreases in intrinsic viscosity. Here, we report a further modification of the previously develop OSF model in an attempt to account for polyion expansion and/or contraction based on the relative amounts of positive and negative charge present on the polyion.

Since our last report, we have experimentally measured intrinsic viscosities over ranges of solution ionic strengths for several copolymers of acrylamide synthesized and characterized in our laboratories. These include different polyelectrolytes and one polyampholyte, all varying in copolymer composition. The collected data has been treated according to the OSF analysis and compared to the data obtained from the literature.

In addition to the previous OSF model, we have explored a new way of modeling polyelectrolyte solution behavior. This is based on rubber elasticity theory developed by Flory to describe the swelling behavior of an electrostatic gel or a loosely crosslinked polymer network containing fixed electrostatic charges.⁷⁹ In this report we provide an interpretation of Flory's theory that can be applied to dilute solutions of polyions. The data from the literature as well as

the data collected in our laboratories has been analyzed and discussed in terms of the Flory model.

Polyion Charge Distribution

Polyions that contain only positive or only negative charges are referred to as polyelectrolytes. The fluid viscosities of polyelectrolyte solutions increase as the solvent electrolyte concentration increases.

Polyions that contain both positive and negative charges are referred to as polyampholytes. Depending on polyion charge composition, the fluid viscosities of polyampholyte solutions can increase or decrease as the solvent electrolyte concentration increases. The effect of charge composition on polyampholyte solution viscosity behavior can be described by defining f as the monomer mole fraction of the most abundant charged monomer in the polymer and g as the monomer mole fraction of the less abundant and oppositely charged monomer in the polymer. Thus, f is greater than or equal to g . The remaining mole fraction of neutral monomer in the polymer is $(1 - f - g)$.

If the charged monomers are randomly placed in the polyampholyte, the charges are geometrically distributed along the polymer chain, and the average spacing between all charges, b , is the monomer length, l_m , divided by the sum of f and g . See Equation (7). It is assumed that all monomers, charged or neutral, have the same length in the polymer chain, l_m .

$$b = \frac{l_m}{f + g} \quad (7)$$

The net amount of charges involved in electrostatic repulsion on the polyampholyte is expected to be proportional to the fraction of charged monomers in excess. This is the difference between f and g . Thus, the net fraction of charged monomers involved in repulsion is $k_c (f - g) / (f + g)$ where k_c is a proportionality constant that is expected to have a value close to unity. The remaining fraction of charged monomers, $1 - [k_c (f - g) / (f + g)] = [(f + g) - k_c (f - g)] / (f + g)$, is involved in the electrostatic attractive forces on the polyampholyte. Thus, the mole fraction of polymer monomer involved in repulsion is $k_c (f - g)$ and the mole fraction of polymer monomers involved in attraction is $[(f + g) - k_c (f - g)]$. The average spacing between net repulsive charges, b_{rep} , is $l_m / [k_c (f - g)] = b (f + g) / [k_c (f - g)]$ and the average charge spacing between net attractive charges, b_{att} , is $l_m / [(f + g) - k_c (f - g)] = b (f + g) / [(f + g) - k_c (f - g)]$. As shown, these effective distances between repulsive and attractive charges can be expressed in terms of the average charge spacing between all charges, b .

Modification of the OSF Model to Include Polyampholyte Solutions

Electrostatic repulsive forces between charged monomers in the polymer expand polymer coil size or increase the intrinsic viscosity. In contrast, the electrostatic attractive forces between monomer charges reduce polymer coil size or decrease the intrinsic viscosity. The OSF model for intrinsic viscosities of polyelectrolyte solutions, developed in the last report, can now be modified to apply to polyampholyte solutions. This modification involves the partitioning of the electrostatic term of Equation (12) in the last report into the sum of a repulsive term, which increases intrinsic viscosity, and an attractive term, which decreases intrinsic viscosity. Equation

(12) and its modification, Equation (8), are shown below. In Equation (8), η_{intr} is the polymer solution intrinsic viscosity, η_{intrHS} is the intrinsic viscosity in absence of electrostatic forces (a condition met at high added salt concentrations), Φ_o is Flory's constant, M is weight average polymer molecular weight, k is a constant of proportionality, l_B is the Bjerrum length, m_o is the average monomer molecular weight, and L_{screen} is the Debye-Hückel screening length.

$$\eta_{\text{intr}}^{\frac{2}{3}} = \eta_{\text{intrHS}}^{\frac{2}{3}} + \frac{l_m \Phi_o^{\frac{2}{3}} M^{\frac{1}{3}} k l_B}{2 m_o} \frac{L_{\text{screen}}}{b} \quad (12) \Leftarrow \text{from last report}$$

$$\eta_{\text{intr}}^{\frac{2}{3}} = \eta_{\text{intrHS}}^{\frac{2}{3}} + \frac{l_m \Phi_o^{\frac{2}{3}} M^{\frac{1}{3}} k l_B}{2 m_o} \frac{L_{\text{screen}}}{b_{\text{rep}}} - \frac{l_m \Phi_o^{\frac{2}{3}} M^{\frac{1}{3}} k l_B}{2 m_o} \frac{L_{\text{screen}}}{b_{\text{att}}} \quad (8)$$

After substituting for b_{rep} and b_{att} in terms of the average charge spacing, b , followed by a collection of terms, Equation (8) becomes Equation (9). Note that if g equals zero and k equals 1.0, then Equation (9) reverts to Equation (12).

$$\eta_{\text{intr}}^{\frac{2}{3}} = \eta_{\text{intrHS}}^{\frac{2}{3}} + \frac{l_m \Phi_o^{\frac{2}{3}} M^{\frac{1}{3}} k l_B}{2 m_o} \frac{2 k_c (f - g) - (f + g)}{(f + g)} \frac{L_{\text{screen}}}{b} \quad (9)$$

Note that the charge composition term $[2 k_c (f - g) - (f + g)] / (f + g)$ is now present. This term determines the direction and magnitude that the polyion electrostatic forces have on the intrinsic viscosity.

The electrostatic term of Equation (9) will be positive if $[2 k_c (f - g) - (f + g)]$ is greater than zero. In this case, the polyion behaves as a polyelectrolyte and the intrinsic viscosity increases as the screening length, L_{screen} , increases. Recall from the last report that the screening length is inversely proportional to the square root of solution ionic strength. Therefore in this case, decreasing a solution's salt concentration increases the intrinsic viscosity.

The electrostatic term of Equation (9) will be zero if $[2 k_c (f - g)]$ equals $(f + g)$. In this case the intrinsic viscosity is not a function of the screening length or the solution's salt concentration.

The electrostatic term of Equation (9) will be negative if $[2 k_c (f - g) - (f + g)]$ is less than zero. In this case, the intrinsic viscosity decreases as the screening length increases and as the solution's salt concentration decreases.

Experimental

Copolymer Synthesis

Acrylamide copolymers were synthesized by free radical polymerization in aqueous solution, the detailed procedure for which has been reported elsewhere.⁸⁰ In general, the appropriate monomers were added to an aqueous 0.5M NaCl solution under light stirring at 30°C. The added NaCl assures random monomer incorporation by screening charged monomers from

one another. Sodium formate, NaOOCH , was added as a chain transfer agent to limit polydispersity. Polymerizations were initiated by VA-044 and allowed to continue for 6 hours. The reactions were then quenched and the polymers were purified by dialysis against deionized H_2O . Monomer structures are shown in Figure 18.

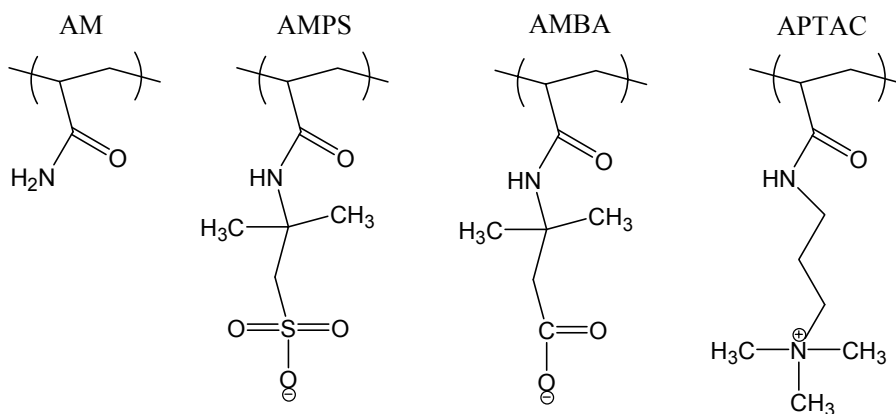


Figure 18. Repeat unit structures in acrylamide copolymers. AM is acrylamide, AMPS is 2-acrylamido-2-methylpropanesulfonate, AMBA is 3-acrylamido-3-methylbutanoate, and APTAC is 3-acrylamidopropyltrimethylammonium

Copolymer Characterization

The adopted polymer nomenclature is indicative of the molar ratio of comonomers fed into the reaction vessel. Actual copolymer compositions were determined by the usual NMR techniques and are reported in the tables below. Polymer molecular weights and polydispersities were determined by GPC using a laser light scattering detector.

Solution Preparation and Characterization

Purified polymer samples were analyzed and corrected for moisture content by drying at 50°C under vacuum overnight. A concentrated master solution was then prepared. Upon complete dissolution, the master solution was diluted to the desired polymer concentration and its ionic strength adjusted by addition of precise amounts of NaCl. The method of isoionic dilution described in our last report was then used to prepare a set of solutions for determining the polymer solution intrinsic viscosity at each ionic strength. Care was taken to ensure that all solutions were in the dilute regime according to restrictions outlined in our last report.

Solution apparent viscosities were measured using the Contraves Low-Shear 30 rheometer at a shear rate of 6s^{-1} and temperature of 25°C. No shear thinning was observed at this low shear rate.

Results and Discussion

Analysis Of Data By The OSF Model

With k_c set to 1, Equation (9) can be rearranged to Equation (10). The left hand side of the equation can be plotted as the ordinate and L_{screen} / b as the abscissa yielding a straight line with a constant slope. The representation of data in this section of this report is a result of this treatment.

$$\left(\frac{\eta_{\text{intr}}^{\frac{2}{3}} - \eta_{\text{intrHS}}^{\frac{2}{3}}}{\frac{1}{M^{\frac{1}{3}}}} \right) \cdot \frac{m_0}{l_m} \cdot \frac{(f + g)}{(f - 3 \cdot g)} = \frac{k \cdot l_B \cdot \Phi_o^{\frac{2}{3}}}{2} \cdot \left(\frac{L_{\text{screen}}}{b} \right) \quad (10)$$

Data gathered from the literature was plotted according to Equation (10) in our last report, and is shown again in Figure 19 for comparison to recently collected data. (Note that since all of the data refers to polyelectrolytes, $g = 0$ and Equation (10) returns to the form last reported.) Details of the specific polymers and their characteristics were given previously. Two apparent trends can be seen in the literature data. Data for the high molecular weight polymers ($M > 300,000$ g/mol) are shown as filled circles in Figure 19. These tend to the middle trend line, regardless of polymer structure. Data for the various lower molecular weight polymers ($M < 300,000$ g/mol) are shown as open circles in Figure 19 and tend to the lower trend line. As expected, both trend lines have intercepts at zero.

The reason that the data forms two lines rather than one is not yet clear. The discrepancy appears to be molecular weight dependent. One possible explanation which we are currently exploring is that the Flory parameter, Φ_o , is not constant for all polymers. Flory developed the parameter for flexible, Gaussian chains. Low molecular weight polymers may violate this condition. Φ_o can be calculated for a given polymer based on its chain diameter, chain length, and persistence or Kuhn length.⁸¹ Future work will determine whether a correction in Φ_o causes a shift of the low molecular weight data onto the center trend line.

As discussed above, intrinsic viscosity data was recently collected over a range of solution ionic strengths for the acrylamide copolymers recently synthesized in our laboratories. All of the copolymer molecular weights exceeded 300,000 g/mole. These data were treated by the OSF model in the same way as the literature data, and results are shown in Figure 19. These results are represented by various symbols to delineate the different copolymer compositions (see Table 7 page 43 for symbol identification).

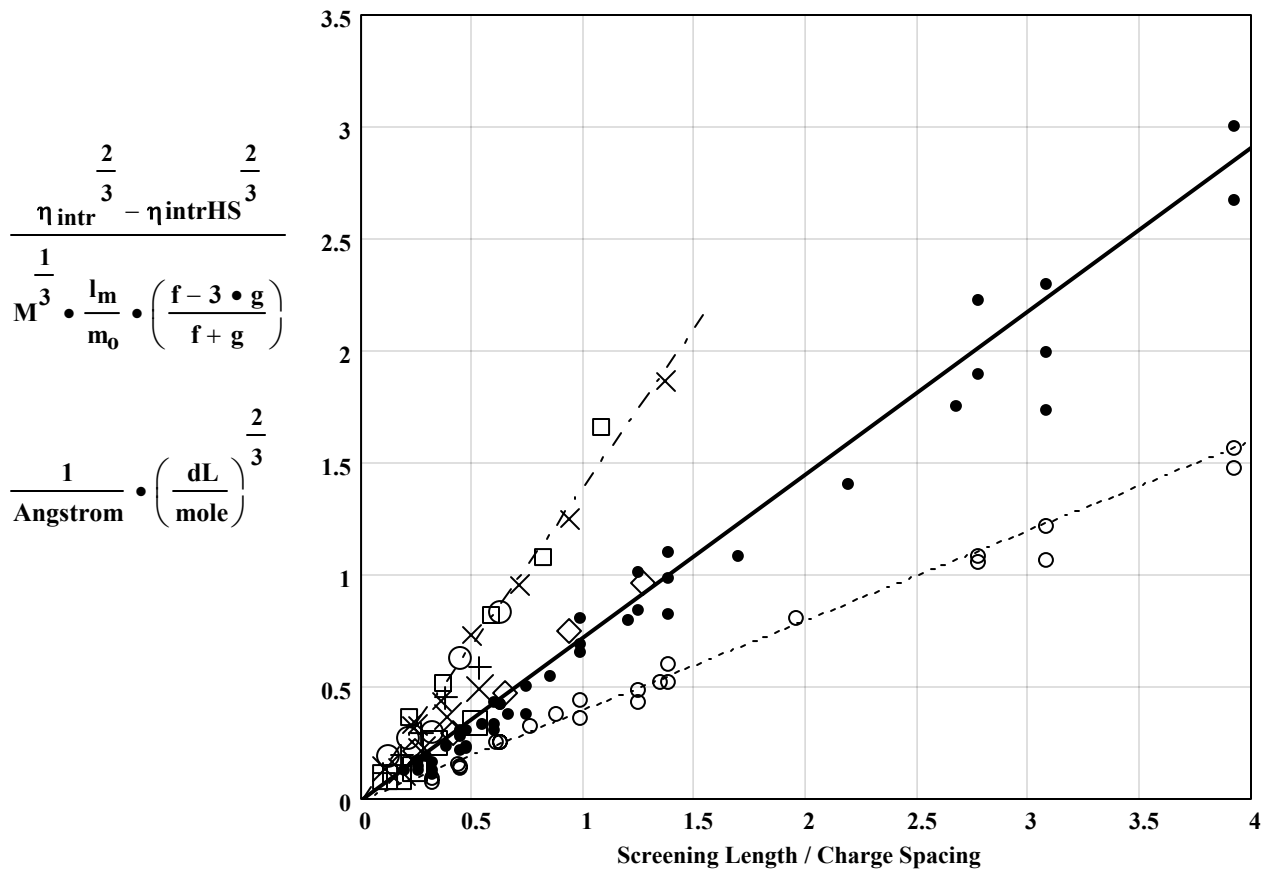


Figure 19. Plot of normalized intrinsic viscosity vs. screening length to charge spacing. Filled circles and solid trend line represent high molecular weight data from the literature. Small open circles and dotted trend line represent low molecular weight data from the literature. Various symbols and dash-dot trend line represent data collected in our laboratory for acrylamide copolymers as identified in Table 7.

The data that we have collected seems to fall into two groups when plotted according to Equation (10). First, the AM:APTAC copolymers, both 5% and 10% incorporation, very nearly follow the middle trend line. Also, data for the terpolymer AM:AMBA:APTAC measured at pH 4 tends to the middle line. This is notable because at pH 4 the AMBA units should be protonated so that only the APTAC units bear charges. It seems that when charged APTAC units are responsible for the electrostatic forces, the data behaves similarly to the literature data for high molecular weight polymers.

The second group of data tends to the upper trend line provided in Figure 19. All of the data in this group are for copolymers in which the charge bearing units are either AMBA or AMPS. Given the similarity of their structures, it is not surprising that these two repeat units have comparable effects on polyion conformation. It is unclear, however, why these copolymers do not behave like the other high molecular weight polymers examined. It is again possible that Φ_0 differs for these polymers, but appropriate calculations must be completed before a conclusion can be reached. Another potential explanation for the difference in this group is that

the Debye-Hückel theory is not valid for the AMBA and AMPS solutions. In these two structures, the negative charge is delocalized over two and three oxygen atoms, respectively. This may result in electrostatic forces that differ substantially from the Debye-Hückel approximation which treats the charges as point charges. Finally, past research has suggested that intramolecular hydrogen bonding can occur between an AMBA or AMPS unit and a neighboring AM unit, stiffening the molecule. One or more of these factors may cause the behavior observed for these copolymers. We are currently working to resolve this issue.

Flory Gel Network Model Applied to Single Polyions

Paul Flory described swelling of a polymer network by solvent as the result of an increase in entropy resulting from mixing solvent and polymer.⁷⁹ The swelling produces elongated polymer configurations that generate elastic forces, thus restricting the degree of network swelling. Eventually an equilibrium degree of swelling is reached in which the expansion and restriction forces are equal. If the polymer has charges, the swelling forces are altered because of electrostatic interactions between polyion charges.

Based on the above mechanism, Flory developed a relationship in which the degree of network swelling, $q_m = V/V_o$ can be determined. V is the molar volume of the swollen polymer network and V_o is molar volume of the unswollen polymer network. In this model development, it was assumed that the degree of polymer crosslinking in the network was small and that the polyion network was in a good solvent containing electrolyte. In the discussion below, Flory's relationship was modified to model the swelling volume of a polymer network composed of a single polyion molecule in a good solvent.

Following Flory's approach, the degree of swelling, q_m , can be expressed by Equation (11) where q_{ma} is the degree of swelling in the absence of electrostatic forces ($q_{ma} = V_a / V_o$ where V_a is the network volume in the absence of electrostatic forces), q_{mrep} is the degree of swelling due to electrostatic repulsion forces, and q_{matt} is the degree of swelling due to electrostatic attractive forces.

$$q_m^{\frac{5}{3}} = q_{ma}^{\frac{5}{3}} + q_{mrep}^{\frac{5}{3}} - q_{matt}^{\frac{5}{3}} \quad (11)$$

Equation (11) can be arranged to give Equation (12). The ratio of q_m to q_{ma} is equal to the ratio of the swollen network molar volume, V , to the network volume in the absence of electrostatic forces, V_a . This ratio is also equal to the ratio of the swollen intrinsic viscosity, η_{intr} , to the unswollen intrinsic viscosity in the absence of electrostatic effects. At high salt concentration, the polyion charges are screened by electrolytes and the intrinsic viscosity at high salt conditions, η_{intrHS} , is expected to represent the network intrinsic viscosity in the absence of electrostatic forces. Using these relationships, Equation (12) can be expressed as Equation (13).

$$\left(\frac{q_m}{q_{ma}} \right)^{\frac{5}{3}} = 1 + \left(\frac{q_{mrep}}{q_{ma}} \right)^{\frac{5}{3}} - \left(\frac{q_{matt}}{q_{ma}} \right)^{\frac{5}{3}} \quad (12)$$

$$\left(\frac{\eta_{intr}}{\eta_{intrHS}} \right)^{\frac{5}{3}} = 1 + \left(\frac{q_{mrep} V_o}{V_a} \right)^{\frac{5}{3}} - \left(\frac{q_{matt} V_o}{V_a} \right)^{\frac{5}{3}} \quad (13)$$

Flory's $q_{mrep}^{5/3}$ and $q_{matt}^{5/3}$ values for a polymer network composed of a single polyion are given by Equations (14) and (15) where Z_p is the number of charges on the polymer chain, and I is the ionic strength of the solution. Using Equations (14) and (15) in Equation (13) and collecting terms gives Equation (16).

$$q_{mrep}^{\frac{5}{3}} = \frac{Z_p^2}{4 V_o I} \left(\frac{k_c (f - g)}{f + g} \right)^2 \quad (14)$$

$$q_{matt}^{\frac{5}{3}} = \frac{Z_p^2}{4 V_o I} \left(1 - \frac{k_c (f - g)}{f + g} \right)^2 \quad (15)$$

$$\left(\frac{\eta_{intr}}{\eta_{intrHS}} \right)^{\frac{5}{3}} = 1 + \frac{Z_p^2 V_o^{\frac{5}{3}}}{4 V_o I V_a^{\frac{5}{3}}} \left(\frac{2 k_c (f - g) - (f + g)}{f + g} \right) \quad (16)$$

But $Z_p = (M l_m) / (m_o)$ b). The ionic strength, I , can be expressed in terms of the screening length, L_{screen} , and Bjerrum length, l_B , as $I = 1/(8 \pi N_A l_B L_{screen}^2)$ where N_A is Avogadro's number. The network volume in the absence of electrostatic forces, V_o , is equal to the product of the polymer molecular weight, M , and the intrinsic viscosity under high salt conditions, η_{intrHS} , where electrostatic forces are screened by the abundance of electrolytes in solution. Using these relationships Equations (16) yields Equation (17).

$$\eta_{intr}^{\frac{5}{3}} = \eta_{intrHS}^{\frac{5}{3}} + \left[\frac{2 \pi N_A l_B l_m^2 V_o^{\frac{2}{3}} M^{\frac{1}{3}}}{m_o^2} \left(\frac{2 k_c (f - g) - (f + g)}{f + g} \right) \right] \left(\frac{L_{screen}}{b} \right)^2 \quad (17)$$

Equation (17) shows that a plot of $\eta_{intr}^{5/3}$ versus $(L_{screen} / b)^2$ should be a straight line. The intercept of the line is equal to $\eta_{intrHS}^{5/3}$ and the slope of the line is equal to the right term of Equation (17) that is enclosed in brackets. In general, the only unknown within the brackets is V_o , the unswollen polymer network molar volume. Thus, the intercept can be used to find η_{intrHS} and the slope of the line can be used to calculate V_o . The two parameters V_o and η_{intrHS} characterize a polyion's intrinsic viscosity response to variations in solution ionic strength or salt concentration. Note that the value of charge composition term, $\{[2 k_c (f - g) - (f + g)] / (f + g)\}$, determines if the intrinsic viscosity increases or decreases with solution ionic strength. Therefore, Equation (17) applies to both polyelectrolytes and polyampholytes. Equation (17) will be used to analyze several sets of experimental data in which a polyion's intrinsic viscosity values were measured as solution ionic strength was varied.

Examination of Polyion Intrinsic Viscosity Data Using the Flory Model

Both data from the scientific literature and recent data obtained in our laboratory were used to examine the performance of the modified Flory model. All experimental data were found to satisfactorily fit the Flory model.

Use of Literature Data

Several sets of polyion intrinsic viscosity data versus solution electrolyte composition were obtained from the literature.⁸²⁻⁸⁷ Details about this data can be found in the last report. Table 8 summarizes properties for each data set. Each data set was plotted as suggested by Equation (17) and the parameters η_{intrHS} and V_o were calculated from the intercept and slope of a line fitted to the data. These parameters are listed in Table 8. All linear fits of the data had good correlations.

Figure 20 shows the intrinsic viscosity to the 5/3 power of each polyion type plotted against the square of the ratio of screening length to average charge spacing using log-log axes. A log-log plot was used to more adequately show all the data. The fit function intrinsic viscosity values for each polyion appear as curved lines. The curved lines would be straight lines if the plot used linear axes. All polyions had a g value of zero.

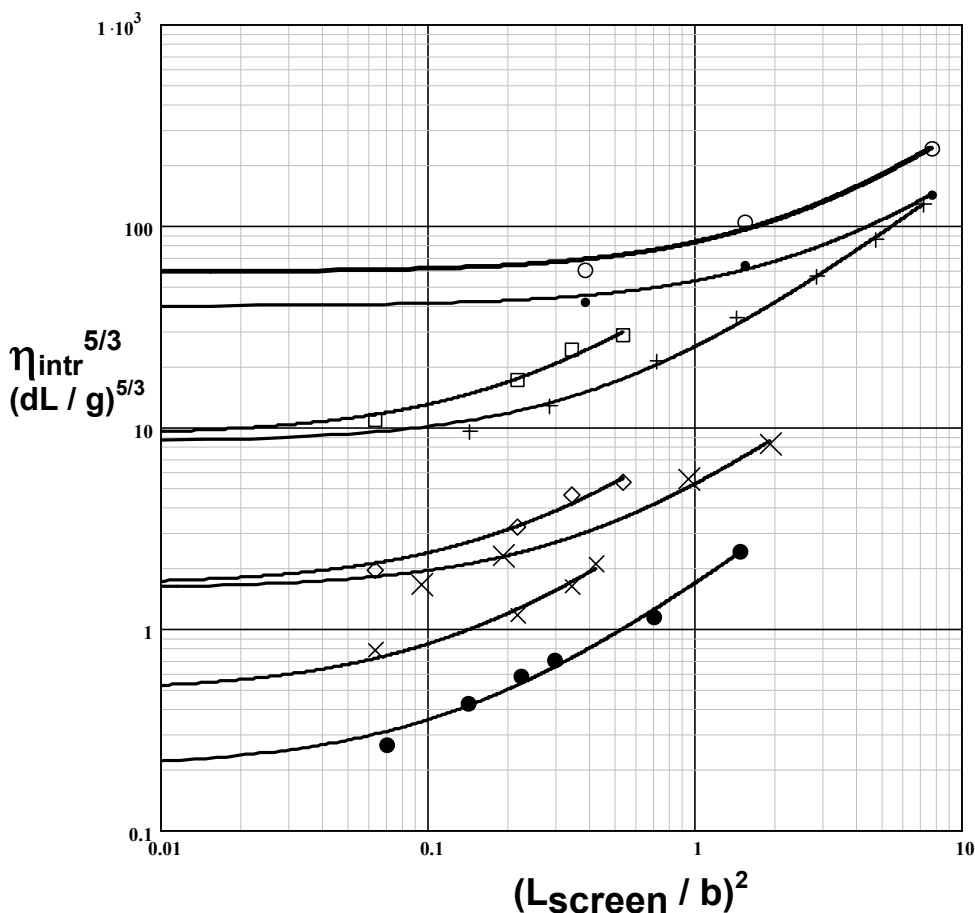


Figure 20: Literature Data and Flory Fit Lines
See Table 8 for data identification.

Table 7: Experimental Information for Laboratory Data

Polyion	Figure 2 Symbol	M g/mole $\times 10^{-6}$	m_o g/mole	f	g	b Å	η_{intrHS} dL / g	V_o liter/mole $\times 10^{-3}$
AM:AMBA=90:10	□	1.09	80.7	0.098	0.000	10.2	5.52	1.98
AM:AMBA=95:05	+	1.05	75.3	0.043	0.000	23.3	4.83	1.96
AM:AMPS=95:05	○	1.00	77.8	0.050	0.000	20.0	5.95	1.94
AM:AMPS=90:10	×	1.10	84.6	0.100	0.000	10.0	6.25	2.19
AM:AMBA:APTAC = 90:05:05 (a)	□	1.51	79.9	0.046	0.043	11.2	5.71	0.048
AM:AMBA:APTAC = 90:05:05 (b)	◇	1.51	79.9	0.043	0.000	21.7	4.72	0.401
AM:APTAC=95:05	X	0.89	75.4	0.044	0.000	57.7	3.54	9.67
AM:APTAC=90:10	◇	0.89	81.7	0.107	0.000	23.4	2.99	2.86

Use of Laboratory Data

Several polyions synthesized at the University of Southern Mississippi by the McCormick research group were examined for intrinsic viscosity properties as a function of solution ionic strength. The data sets were analyzed using the Flory model. Each data set was plotted as suggested by Equation (17) and the parameters η_{intrHS} and V_o were calculated from the intercept and slope of a straight line fitted to the data using a k_c value of unity. These parameters are listed in Table 7. All fits of the data to a straight line had good correlations.

Figure 21 shows the intrinsic viscosity to the 5/3 power of each polyion type plotted against the square of the ratio of screening length to average charge spacing using log-log axis. A log-log plot was used to more adequately show all the data. The fit function intrinsic viscosity values for each polyion are shown as curved lines. The monomer length, l_m , for all the laboratory polyions was 2.56 Å.

Table 8: Experimental Information for Literature Data

Polyion	Reference Number	Figure 1 Symbol	M g/mole $\times 10^{-6}$	m_o g/mole	b Å	l_m Å	η_{intrHS} dL / g	V_o liter/mole $\times 10^{-3}$
NaCMC (a)	83	○	1.06	247	11.0	5.15	11.5	9.12
NaCMC (b)	83	•	0.75	247	11.0	5.15	9.13	4.49
AM:CMA=70:30	84	+	1.44	97.1	11.4	2.56	3.60	2.23
PAA	85	●	0.048	71.5	7.16	2.56	0.39	0.14
HPAM (a)	86	×	0.156	71.0	35-14	2.56	0.65	0.26
HPAM (b)	86	◇	0.382	71.0	35-12	2.56	1.35	0.49
HPAM (c)	86	□	1.14	71.0	35-12	2.56	3.77	3.42
AMPS	87	X	0.86	207	9.9	2.56	1.32	2.86

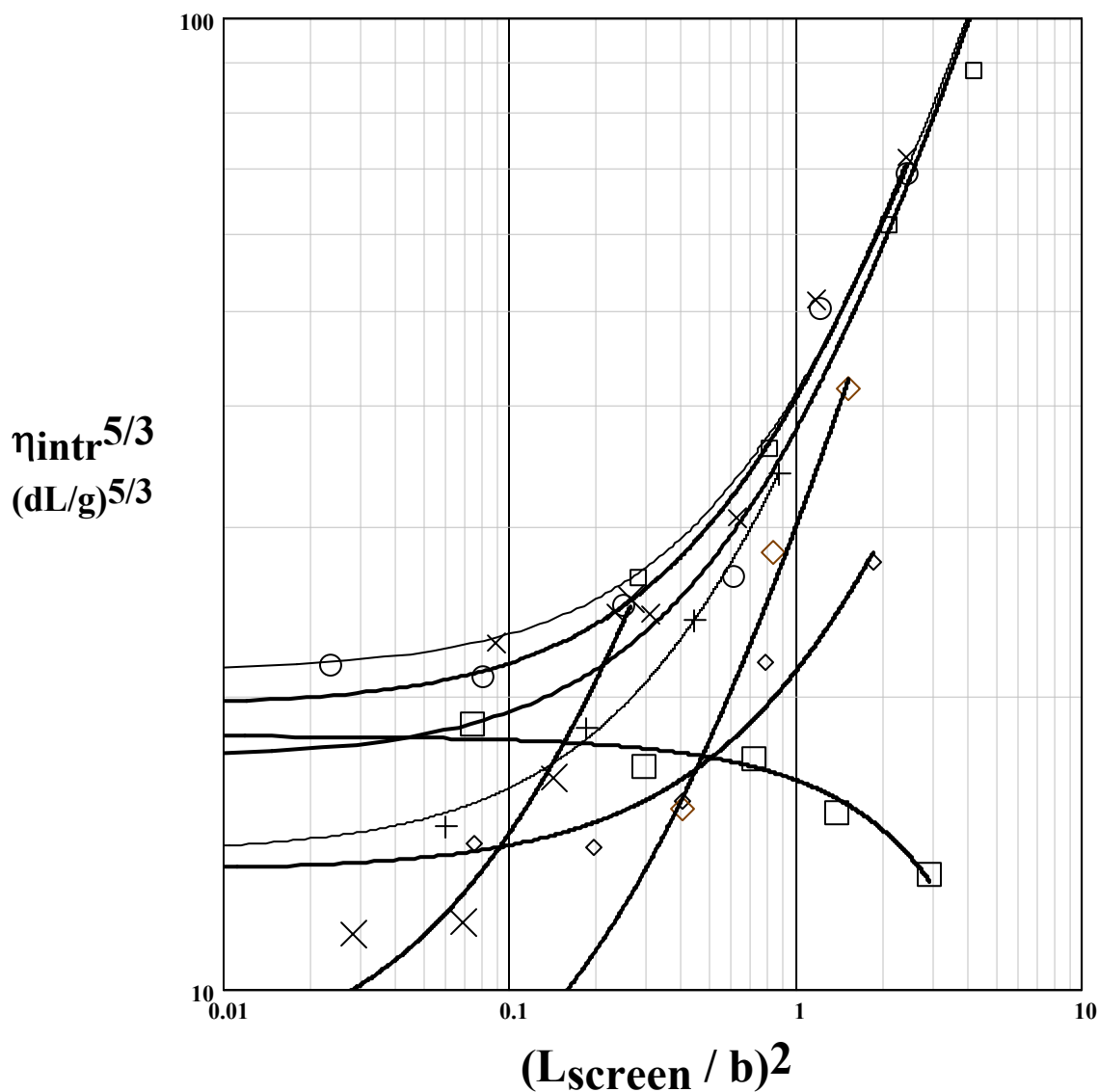


Figure 21: Laboratory Data and Flory Fit Lines
See Table 8 for data identification.

Discussion of Modified Flory Model

Both the literature and laboratory data sets appear to fit the modified Flory model. The data for each polyion, when plotted as $\eta_{intr}^{5/3}$ versus $(L_{screen} / b)^2$, fit a straight line with a reasonably good correlation. The intrinsic viscosities, in the absence of electrostatic forces and obtained from the plot intercepts, had reasonable values for each polyion. The molar volumes of the unswollen polymer obtained from the plot slopes had a wide range of values. The values of the molar volume of the unswollen polymer could not be correlated with polyion molecular weight or charge spacing. Because this parameter has such a large variation of values with no

apparent correlation to polyion structure, this fitting parameter cannot be assigned a physical or structural meaning at this time.

Conclusions

A successful polymer flooding process relies on polymer solution extensional viscosity which has been found to correlate with solution intrinsic viscosity. Therefore, a universal model describing polymer solution intrinsic viscosity dependence on polymer and solvent properties would be especially useful in polymer flooding design. With a dependable model, polymer floods could be formulated to maximize viscosity at reservoir conditions and maintain oil displacement efficiency.

Because polyions are of immediate interest, modifications to two polyion solution theories were made, and the two resulting models were studied to understand their predictive capabilities. A modified OSF model and a model derived from the work of Flory were developed. Polyelectrolyte solution intrinsic viscosity information collected from the scientific literature and recent polyion solution data obtained in our laboratories were analyzed using both models. Both models were successfully fit to solution intrinsic viscosity data over ranges of solution ionic strengths.

The modified Flory model fit both the literature and laboratory data sets. Each polyion generated a unique model parameter, the molar volume of the unswollen polymer. However, parameter values could not be correlated with individual polyion physical properties such as macromolecular structure or molecular weight. Thus, at this time, the Flory model does not appear to provide a universal relationship between polymer solution viscosities and polymer and solvent properties.

When the solution data was plotted using the OSF model, three distinct lines were formed. The reason that the data forms three lines rather than one universal line appears to be molecular weight dependent. One possible explanation is that the OSF model was derived for high molecular weight polymers that form flexible Gaussian chains. Depending on macromolecular structure, low molecular weight polymers may violate this condition and thus produce a different correlation line when plotted. Future work will determine whether a model correction for polymer molecular weight will shift all of the data onto a single trend line.

Nomenclature

Symbol	Dimension	Description
b	Å	Average distance between polyion charges
b_{att}	Å	Distance between opposite polyion charges
b_{rep}	Å	Distance between like polyion charges
f	dimensionless	Mole fraction of more abundant charged monomer
g	dimensionless	Mole fraction of less abundant charged monomer
I	mole / liter	Solution ionic strength
k	dimensionless	Constant of proportionality in OSF model
k_c	dimensionless	Constant of proportionality in Flory model
L_{screen}	Å	Debye-Hückel screening length
l_B	Å	Bjerrum length
l_m	Å	Monomer length
M	g / mole	Polymer molecular weight
m_o	g / mole	Monomer molecular weight
N_A	1/mole	Avogadro's number, 6.02×10^{23} per mole
q_m	dimensionless	Total degree of network swelling
q_{ma}	dimensionless	Network swelling without electrostatic forces
q_{matt}	dimensionless	Network swelling due to electrostatic attractions
q_{mrep}	dimensionless	Network swelling due to electrostatic repulsions
V	dL/mole	Molar volume of swollen polymer network
V_a	dL/mole	Molar network volume without electrostatic forces
V_o	dL/mole	Molar volume of unswollen polymer network
Z_p	dimensionless	Number of charges on a single polyion
Φ_o	1/mole	Flory constant for flexible coils, 2.86×10^{23} /mole
η_{intr}	dL/g	Polymer solution intrinsic viscosity
η_{intrHS}	dL/g	Polymer solution intrinsic viscosity without electrostatic forces (high salt concentration)

References

- ¹ Lowe, A. B. and McCormick, C. L. *Chem. Rev.* **2002**, 102(11), 4177-4189.
- ² Morawetz, H. *Macromolecules in Solution*, 2nd Ed. Robert E. Krieger Publishing Co.: Malabar, FL, 1983, p. 315.
- ³ Bekturov, E. A.; Kudaibergenov, S. E.; Rafikov, S. R. *Macromol. Chem. Phys.* **1990**, C30, 233.
- ⁴ Hart, R.; Timmerman, D. J. *Polymer Sci.* **1958**, 28, 638.
- ⁵ Schulz, D. N.; Peiffer, D. G.; Agarwal, P.K.; Larabee, J.; Kaladas, J. J.; Soni, L.; Handwerker, B.; Garner, R. T.; *Polymer* **1986**, 27, 1734.
- ⁶ Schulz, D. N.; Kitano, K.; Danik, J.A.; Kaladas, J. J. *Polym. Mat. Sci. Eng.* **1987**, 147, 149.
- ⁷ Huglin, M.B.; Radwan, M.A. *Polymer International* **1991**, 26, 97.
- ⁸ Konack, C.; Rath, R. C.; Kopeckova, P.; Kopecek, J. *Polymer* **1993**, 34, 4767.
- ⁹ Konack, C.; Rath, R. C.; Kopeckova, P.; Kopecek, J. *Macromolecules* **1994**, 27, 1992.
- ¹⁰ Monroy Soto, V. M.; Galin, J. C. *Polymer* **1984**, 25, 121.
- ¹¹ Monroy Soto, V. M.; Galin, J. C. *Polymer* **1984**, 25, 254.
- ¹² Wielemans, T. A., Engberts, J. B. F. N. *European. Polymer Journal* **1987**, 23, 947.
- ¹³ Kathmann, E. E.; Davis, D. D.; McCormick, C. L. *Macromolecules* **1994**, 27, 3156.
- ¹⁴ Lee, W-F.; Tsai, C-C *Polymer* **1995**, 36, 357.
- ¹⁵ Salamone, J. C.; Volksen, W.; Israel, S.C.; Olson, A. P.; Raia, D. C. *Polymer* **1977**, 18, 1058.
- ¹⁶ Salamone, J. C.; Volksen, W.; Olson, A. P.; Israel, S.C. *Polymer* **1978**, 19, 1157.
- ¹⁷ Wielemans, T. A.; Engberts, J. B. F. N. *European Polymer Journal*, **1990**, 26, 639.
- ¹⁸ Lowe, A.B., Billingham, N.C., and Armes, S.P. *Macromolecules*, **1999**, 32, 2141.
- ¹⁹ Lowe, A.B., Billingham, N.C., and Armes, S.P. *Macromolecules* **1998**, 31, 5991.
- ²⁰ Candau, F. Regalado, E. J.; Selb E. J., *Macromol. Sym.* **2000**, 150, 241-249.
- ²¹ McCormick, C. L.; Middleton, J. C.; and Grady, C. E. *Polymer* **1992**, 33, 4184.
- ²² Middleton, J. C. *Ph.D. Dissertation*, University of Southern Mississippi, 1990.
- ²³ Branham, K. D. *Ph.D. Dissertation*, University of Southern Mississippi, 1995.
- ²⁴ Branham, K. D.; Snowden, H. S.; McCormick, C. L. *Macromolecules* **1996**, 29, 254.
- ²⁵ Smith, G. L. and McCormick, C. L. *Macromolecules* **2001**, 34, 918.
- ²⁶ Smith, G. L. and McCormick, C. L. *Macromolecules* **2001**, 34, 5579.
- ²⁷ Smith, G. L. and McCormick, C. L. *Langmuir* **2001**, 17, 1719.
- ²⁸ Paleos, M. C. in *Polymerization in Organized Media*; Paleos, M. C., Ed.; Gordon and Breach Science: Philadelphia, **1992**; Chapter 3, 183.
- ²⁹ Candau, F.; Zana, R. in *Polymeric Materials Encyclopedia*; Salamone, J. C., Ed.; CRC: Boca Raton, FL, **1996**; Vol. 6, 4287.
- ³⁰ Laschewsky, A. *Adv. Polym. Sci.* **1995**, 124, 1.
- ³¹ Nagai, K. *Trends Polym. Sci.* **1996**, 4, 122.
- ³² Strauss, U. P.; Gershfeld, N. L. *J. Phys. Chem.* **1954**, 58, 747.
- ³³ Dubin, P.; Strauss, U. P. *J. Phys. Chem.* **1970**, 74, 2842.
- ³⁴ Strauss, U.; Vesnaver, G. *J. Phys. Chem.* **1975**, 79, 1558.
- ³⁵ Strauss, U. P.; Schlesinger, M. S. *J. Phys. Chem.* **1978**, 82, 1627.
- ³⁶ Ezzell, S. A.; McCormick, C. L. *Macromolecules* **1992**, 25, 1881.
- ³⁷ Ezzell, S. A.; McCormick, C. L. *Macromolecules* **1992**, 25, 1887.
- ³⁸ McCormick, C. L.; Middleton, J. C.; Cummins, D. F. *Macromolecules* **1992**, 25, 1201.
- ³⁹ Chang, Y.; McCormick, C. L. *Macromolecules* **1993**, 26, 6121.

- 40 Hu, Y.; Smith, G. L.; Richardson, M. F.; McCormick, C. L.; *Macromolecules* **1997**, *30*, 3526.
- 41 Hu, Y.; Armentrout, R. S.; McCormick, C. L. *Macromolecules* **1997**, *30*, 3538.
- 42 Morishima, Y. *Prog. Polym. Sci.* **1990**, *15*, 949.
- 43 Morishima, Y. *Adv. Polym. Sci.* **1992**, *104*, 51.
- 44 Morishima, Y. *Trends Polym. Sci.* **1994**, *2*, 31.
- 45 Morishima, Y. in *Multidimensional Spectroscopy of Polymers: Vibrational, NMR, and Fluorescence Techniques*; Urban, M. W.; Provder, T., Eds.; ACS Symposium Series 598; American Chemical Society; Washington, DC, **1995**; 490.
- 46 Torstensson, M.; Rånby, B.; Hult, A. *Macromolecules* **1990**, *23*, 126.
- 47 Stähler, K.; Selb, J.; Barthelémy, P.; Puci, B.; Candau, F. *Langmuir*
- 48 Chang, Y.; McCormick, C. L. *Polymer* **1994**, *35*, 3503.
- 49 Ueda, T.; Harada, S.; Ise, N. *Poly. J.* **1974**, *6*, 473.
- 50 Ringsdorf, H.; Schlarb, B.; Venzmer, J. *Angew. Chem. Int. Engl. Ed.* **1988**, *27*, 113.
- 51 Butler, G. B.; Do, C. H. in *Water-Soluble Polymers*; Shalaby, S. W., McCormick, C. L., Butler, G. B., Eds.; ACS Symposium Series 467, American Chemical Society, Washington, DC, **1991**, 151.
- 52 Butler, G.B., and Angelo, R.J. *J. Am. Chem. Soc.*, **1957**, *79*, 3128.
- 53 Goethals, E.J. ed. *Polymeric Amines and Ammonium Salts* Pergamon Press, Oxford. **1979** and references therein.
- 54 Butler, G.B. ed. *Cyclopolymerization and Cyclocopolymerization* Marcel Dekker: New York. **1992** and references therein.
- 55 Berry, G. C. *J. Chem. Phys.* **1966**, *44*, 4550.
- 56 Rietveld, I. B., Smit, J. A. M. *Macromolecules* **1999**, *32*, 4608.
- 57 Galinsky, G., Burchard, W. *Macromolecules* **1997**, *30*, 4445.
- 58 Anthony, O.; Zana, R. *Langmuir* **1996**, *12*, 1967.
- 59 Maruthamuthu, M.; Subramanian, E. *Colloid and Polymer Science* **1990**, *268*, 256.
- 60 Christian, S. D.; Scamehorn, J. F. (Eds.) *Solubilization in Surfactant Aggregates*; Marcel Dekker, Inc.: New York City, New York, **1995** and references therein.
- 61 Lancaster, J.E., Baccei, L., Panzer, H.P. *Polymer Letters*, **1976**, *14*, 549.
- 62 Lancaster, J. E.; Baccei, L.; Panzer, H. P. *Polymer Letters*, **1976**, *14*, 549.
- 63 Tidwell, P.W., and Mortimer, G.A. *J. Polym. Sci.: Part A* **1965**, *2*, 369.
- 64 Tidwell, P. W.; Mortimer, G. A. *J. Polym. Sci.: Part A* **1965**, *2*, 369.
- 65 Igarahi, S. *J. Polym. Sci. Polym. Lett. Ed.* **1963**, *1*, 359.
- 66 Galin, M., Chapoton, A., Galin, J. C. *J. Chem. Soc. Perkin Trans.* **1993**, *2*, 545
- 67 Higgs, P. G.; Joanny, J.-F. *J. Chem. Phys.* **1991**, *94*, 1543.
- 68 Candau, F.; Joanny, J. -F. *Polyampholytes (Properties in Aqueous Solution)*; Salamone, J. C., Ed.; CRC Press: Boca Raton, FL 1996, Vol. 7.
- 69 Wittmer, J.; Johner, A.; Joanny, J.-F. *Europhys. Lett.* **1993**, *24*, 263.
- 70 Everaers, R.; Johner, A.; Joanny, J.-F. *Europhys. Lett.* **1997**, *37*, 275.
- 71 Katchalsky, A.; Spitnik, P. *J. Poly. Sci.* **1947**, *2*, 432.
- 72 Armentrout, R. S.; and McCormick, C. L. *Macromolecules* **2000**, *33*, 419.
- 73 Top, A.; Belkoura, L.; Woermann, D. *Macromolecules* **1996**, *29*, 5392.
- 74 Forster, S.; Schmidt, M. *Adv. Poly. Sci.* **1995**, *120*, 53.
- 75 Beer, M.; Schmidt, M.; Muthukumar, M. *Macromolecules* **1997**, *30*, 8375.

- ⁷⁶ Bhat, S. N.; Smith, G. A.; Tucker, E. E.; Christian, S. D.; Scamehorn J. F.; Smith, W. *Industrial Engineering Chemical Research* **1987**, *26*, 1217.
- ⁷⁷ Rushing, T.S., Hester, R. D., *J. Appl. Polym. Sci.*, **2003**, *89*(10), 2831-2835.
- ⁷⁸ Semi-Annual Report, Stimuli Responsive Polymers, DOE DE-FC26-01BC15317 R03.
- ⁷⁹ Flory, P.J., *Principles of Polymer Chemistry*, Cornell Univ. Press: New York, 1953.
- ⁸⁰ Fevola, Michael, Bridges, J. K., Kellum, M. G., Hester, R. D., McCormick, C. L., accepted for publication in *J. Appl. Polym. Sci.*, September 2003.
- ⁸¹ Yamakawa, A.; Fujii, M.; *Macromolecules* **1974**, *7*, 128-135.
- ⁸² Brown, W.; Henley, D.; *Makromol. Chem.* **1964**, *79*, 68-88.
- ⁸³ Mabire, F.; Audebert, R.; Quivoron, C.; *Polymer* **1984**, *25*, 1317-1322
- ⁸⁴ Mylonas, Y.; Staikos, G.; Ullner, M.; *Polymer* **1999**, *40*, 6841-6847.
- ⁸⁵ Kulkarni, R. A.; Gundiah, S.; *Makromol. Chem.* **1984**, *185*, 957-967.
- ⁸⁶ Kulkarni, R. A.; Gundiah, S.; *Makromol. Chem.* **1984**, *185*, 969-982.
- ⁸⁷ Fisher, L.W., Sochor, A. R., Tan, J. S., *Macromolecules* **1977**, *10*(5), 949-954